Inhibiting Insulin-Mediated β_2-Adrenergic Receptor Activation Prevents Diabetes-Associated Cardiac Dysfunction

BACKGROUND: Type 2 diabetes mellitus (DM) and obesity independently increase the risk of heart failure by incompletely understood mechanisms. We propose that hyperinsulinemia might promote adverse consequences in the hearts of subjects with type-2 DM and obesity.

METHODS: High-fat diet feeding was used to induce obesity and DM in wild-type mice or mice lacking β_2-adrenergic receptor (β_2AR) or β-arrestin2. Wild-type mice fed with high-fat diet were treated with a β-blocker carvedilol or a GRK2 (G-protein-coupled receptor kinase 2) inhibitor. We examined signaling and cardiac contractile function.

RESULTS: High-fat diet feeding selectively increases the expression of phosphodiesterase 4D (PDE4D) in mouse hearts, in concert with reduced protein kinase A phosphorylation of phospholamban, which contributes to systolic and diastolic dysfunction. The expression of PDE4D is also elevated in human hearts with DM. The induction of PDE4D expression is mediated by an insulin receptor, insulin receptor substrate, and GRK2 and β-arrestin2-dependent transactivation of a β_2AR-extracellular regulated protein kinase signaling cascade. Thus, pharmacological inhibition of β_2AR or GRK2, or genetic deletion of β_2AR or β-arrestin2, all significantly attenuate insulin-induced phosphorylation of extracellular regulated protein kinase and PDE4D induction to prevent DM-related contractile dysfunction.

CONCLUSIONS: These studies elucidate a novel mechanism by which hyperinsulinemia contributes to heart failure by increasing PDE4D expression and identify β_2AR or GRK2 as plausible therapeutic targets for preventing or treating heart failure in subjects with type 2 DM.

Qingtong Wang, MD, PhD*
Yongming Liu, MD, PhD*
Qin Fu, MD, PhD*
Bing Xu, BS
Yuan Zhang, PhD
Sungjin Kim, PhD
Ruensern Tan, MS
Federica Barbagallo, PhD
Toni West, MS
Ethan Anderson, PhD
Wei Wei, PhD
E. Dale Abel, MB. BS, DPhil
Yang K. Xiang, PhD

*Drs Wang, Liu, and Fu contributed equally.

Correspondence to: E. Dale Abel, MB, BS, DPhil, Department of Medicine, Division of Endocrinology and Metabolism and Fraternal Order of Eagles Diabetes Research Center, University of Iowa, Iowa City, IA 52242 or Yang K. Xiang, PhD, Department of Pharmacology, University of California at Davis, Davis, CA 95616. E-mail DRCAdmin@uiowa.edu or ykxiang@ucdavis.edu

Sources of Funding, see page 86

Key Words: β-adrenergic receptors ■ diabetic cardiomyopathy ■ heart failure ■ insulin ■ phosphodiesterase

Clinical Perspective

What Is New?

- Hyperinsulinemia, which characterizes insulin-resistant states, synergistically interacts with β_2-adrenergic receptor signaling pathways by induction of the phosphodiesterase phosphodiesterase 4D that degrades cAMP. This pathway is activated in human hearts in diabetes mellitus.
- Hyperinsulinemia-induced β_2-adrenergic receptor signaling pathway inhibits cardiac function and promotes structural injury.
- In a mouse model of obesity and type 2 diabetes mellitus, myocardial injury and dysfunction can be reversed by pharmacologically inhibiting GRK2 signaling with the drug Paroxetine (currently used clinically as an antidepressant) or by inhibiting β_2-adrenergic receptor signaling with Carvedilol independently of changes in systemic metabolic parameters (ie, hyperglycemia and hyperinsulinemia).

What Are the Clinical Implications?

- This is the first demonstration that targeting this novel insulin-β_2-adrenergic receptor pathway therapeutically may materially prevent diabetes mellitus-associated heart failure, which remains a clinically intractable problem that may be exacerbated after treatment with most existing diabetes mellitus therapeutics, particularly those that cause hyperinsulinemia.
- This study has significant implications for the use of β-blockers in the management of diabetes mellitus-associated heart failure and opens up a new therapeutic role for an existing drug that could be repurposed to treat heart failure in diabetes mellitus.

Cardiovascular disease remains the greatest unmet challenge in reducing mortality in subjects with type 2 diabetes mellitus (DM) and the metabolic syndrome.[1] Heart failure risk remains substantially elevated in (DM) even after adjusting for traditional risk factors such as ischemic heart disease and hypertension.[2] Indeed, the term diabetic cardiomyopathy has been used to describe intrinsic pathophysiological mechanisms in cardiomyocytes, which are exacerbated by DM, that directly lead to cardiac dysfunction or may exacerbate cardiac dysfunction in the face of stressors such as cardiac ischemia or hypertrophy.[2,3] Multiple mechanisms have been suggested, including altered substrate metabolism, mitochondrial dysfunction, and altered calcium signaling.[4] Altered myocardial insulin signaling has emerged as a potential pathophysiological mechanism.[5,6] The specific mechanisms linking insulin resistance and heart failure have been challenging to unravel given the complex interactions between insulin signaling pathways, such as Akt signaling, chronic activation of which may accelerate ventricular remodeling,[7–9] and impaired activation of FOXO proteins, a hallmark of cellular insulin resistance, which may also exacerbate heart failure in insulin-resistant states.[10–12] Moreover, in type 2 DM, hyperinsulinemia has been associated with depressed adrenergic signaling, which may lead to decreased contractility despite elevated catecholamine levels presumably because of either dysfunctional calcium handling within cardiomyocytes or catecholamine-induced β-adrenergic receptor (βAR) desensitization.[13–16]

Human studies have suggested that insulin receptor (IR)-mediated signaling is enhanced in heart failure.[9] We also recently demonstrated that reducing IR signaling in cardiomyocytes attenuated left ventricular (LV) dysfunction and adverse LV remodeling after transverse aortic constriction.[7] A novel mechanism by which hyperinsulinemia might impair myocardial contractility is by inhibition of adrenergic signaling. We recently provided direct molecular evidence for an inhibitory effect of insulin signaling on β-adrenergic responsiveness in the heart that was mediated by β_2AR signaling pathways.[17] It is interesting to note that some clinical trials have suggested that insulin treatment or drugs that may raise circulating insulin concentrations might increase mortality or hospitalization rates in patients with heart failure.[18–21] Although β blockade with either β-1 selective agents, such as metoprolol[22] or β_1AR, and β_2AR nonselective agents, such as carvedilol,[23] reduces mortality in patients with DM and heart failure, the mortality reduction benefit is attenuated relative to nondiabetics, and some trials suggest that agents with β_2AR-blocking properties could be superior.[24] Therefore, additional mechanistic studies are required to elucidate the complex interactions between insulin and β-adrenergic signaling that may increase heart failure risk in DM.

Biochemically, IRs and βARs induce heterologous signal transduction pathways leading to different cellular processes. IRs, a member of the large receptor tyrosine kinase family, phosphorylates insulin receptor substrate, leading to Akt and extracellular regulated protein kinase (ERK) activation.[25–27] Ligand binding to βARs, which are prototypical members of the G protein-coupled receptor superfamily, induces cAMP-dependent protein kinase A (PKA) activation.[28–31] Studies in adipocytes and liver cells have suggested that insulin and adrenergic stimulation act reciprocally to blunt each other's signaling. Recently, we have shown that IRs and β_2ARs form a membrane receptor complex to coordinate signal transduction induced by insulin and catecholamines in the heart.[17,32] The mechanism and consequence of cross-talk between IRs and βARs appears to be cell- and tissue-specific and remains incompletely understood in cardiac tissue. In particular, little is known about how IR signaling may affect βAR signaling in the myocardium to modulate cardiac function in clinically relevant states, such as DM and heart failure.

We hypothesized that DM-associated heart failure is caused, in part, by decreased myocardial contractility that is mediated by insulin-induced depression of βAR signaling in cardiomyocytes, which decreases cAMP/PKA activities and substrate phosphorylation, which are required to sustain cardiac contractility. In the present study, we reveal that hyperinsulinemia selectively induces cardiac expression of phosphodiesterase 4D (PDE4D), an enzyme that is critically involved in regulating cAMP-PKA activity in cardiac adrenergic signaling and function.[33,34] We show that hyperinsulinemia-induced PDE4D expression impairs adrenergic regulation and promotes cardiac dysfunction in a diabetic model induced by high-fat diet (HFD) feeding and identify the molecular pathways that mediate this. We also demonstrate that pharmacological or genetic inhibition of these pathways can effectively prevent or treat obesity or DM-related heart failure.

METHODS

Experimental Animals and In Vivo Treatment

The animal care and experimental protocols followed US National Institutes of Health guidelines and were approved by the Institutional Animal Care and Use Committees of the University of California at Davis, the University of Utah, and the Carver College of Medicine of the University of Iowa. C57BL/6J mice were purchased from Charles River. Six-week-old male wild-type, β_2AR global knockout (β_2KO), and β-arrestin2 global knockout (β-arr2 KO) mice were randomly assigned to 2 groups fed ad libitum with either a low-fat diet or a matched HFD (Research Diets Inc.) for 6 months (n=26). The low-fat diet was D12450J (3.85 kcal/g; 10% of calories from fat, 20% of calories from protein, and 70% of calories from carbohydrate), and the HFD was D12492 (5.24 kcal/g; 60% of calories from fat, 20% of calories from protein, and 20% of calories from carbohydrate). Blood glucose levels were measured after a fast of 6 hours. Cardiac function was assessed at 4 weekly intervals starting after 8 weeks on on the HFD until 24-weeks, by echocardiography under isoflurane anesthesia. Mice were subjected to intraperitoneal glucose tolerance testing after each echocardiography study. Echocardiography was performed with a Vevo 2100 imaging system from VisualSonics with a 22- to 55-MHz MS550D transducer.

Primary Adult Cardiomyocyte Isolation and Culture

The isolation of adult cardiomyocytes was carried out as described previously.[17] Freshly isolated adult cardiomyocytes were loaded with Fluo-4 AM (5 μM; Molecular Probes) for 30 minutes before measuring calcium transients and contractility as described.[32]

Statistical Analysis

All data are expressed as mean±SEM. All statistical analysis was performed using the SPSS statistical software, version 22.0. The sample size for each group is shown in the figure legends or in the online-only Data Supplement tables. The in vitro studies were done with at least 3 sets of independent experiments. All data were normally distributed. The differences between 2 groups were then evaluated by 2-tailed Student's *t* test, and the comparisons of multiple groups were performed with either 1- or 2-way analysis of variance, followed by post hoc Tukey's test. For the time course animal studies, data were analyzed with repeated measures analysis of variance. $P<0.05$ was defined as statistically significant.

Extended methods can be found in the online-only Data Supplement materials.

RESULTS

We examined whether DM is associated with modification of adrenergic signaling in human hearts. In right atrial appendage tissues from patients with type 2 DM or nondiabetics obtained at the time of coronary artery bypass surgery, PDE, and G-protein-coupled receptor kinase 2 (GRK2) were significantly increased relative to patients without DM (Figure 1A). We then examined a murine model of HFD feeding that develops obesity, hyperglycemia, and hyperinsulinemia (online-only Data Supplement Figure IA and IB). After 6 months of HFD feeding, these animals developed cardiac hypertrophy and fibrosis when compared with normal chow (NC) controls; they also displayed a small but significant increase in apoptosis in myocardium (online-only Data Supplement Figure IIA and IIB). In concordance with data from human tissues, both mRNA and protein levels of a PDE4 family gene PDE4D were specifically induced in HFD hearts relative to those fed with NC (Figure 1B and 1C). In contrast, the other PDE isoforms were not altered (Figure 1C). In isolated adult ventricular myocytes (AVMs), insulin but not glucose, induced PDE4D protein levels (Figure 1D), suggesting that insulin-induced signaling may modulate PDE4D expression in HFD hearts. We also examined insulin-signaling pathways in HFD hearts. The expression of IR and IRS2 were reduced in HFD hearts relative to those fed with NC (Figure 1E and online-only Data Supplement Figure IC). Accordingly, compared with isolated myocytes from NC hearts, myocytes from HFD hearts displayed a blunted response to insulin stimulation (online-only Data Supplement Figure ID). It is important to note that basal ERK and Akt signaling and downstream S6K1 and GSK3 phosphorylation were significantly elevated in HFD hearts relative to those fed with NC (Figure 1E). These data suggest that, despite insulin resistance, ambient hyperinsulinemia may activate the remaining IRs to promote downstream signaling that might regulate gene expression.

PDE4D plays an essential role in controlling cAMP levels in hearts by hydrolysis of cyclic nucleotides. In HFD hearts with elevated PDE4D expression, cAMP levels and cAMP-dependent PKA phosphorylation of substrates such as phospholamban (PLB) and troponin I that are

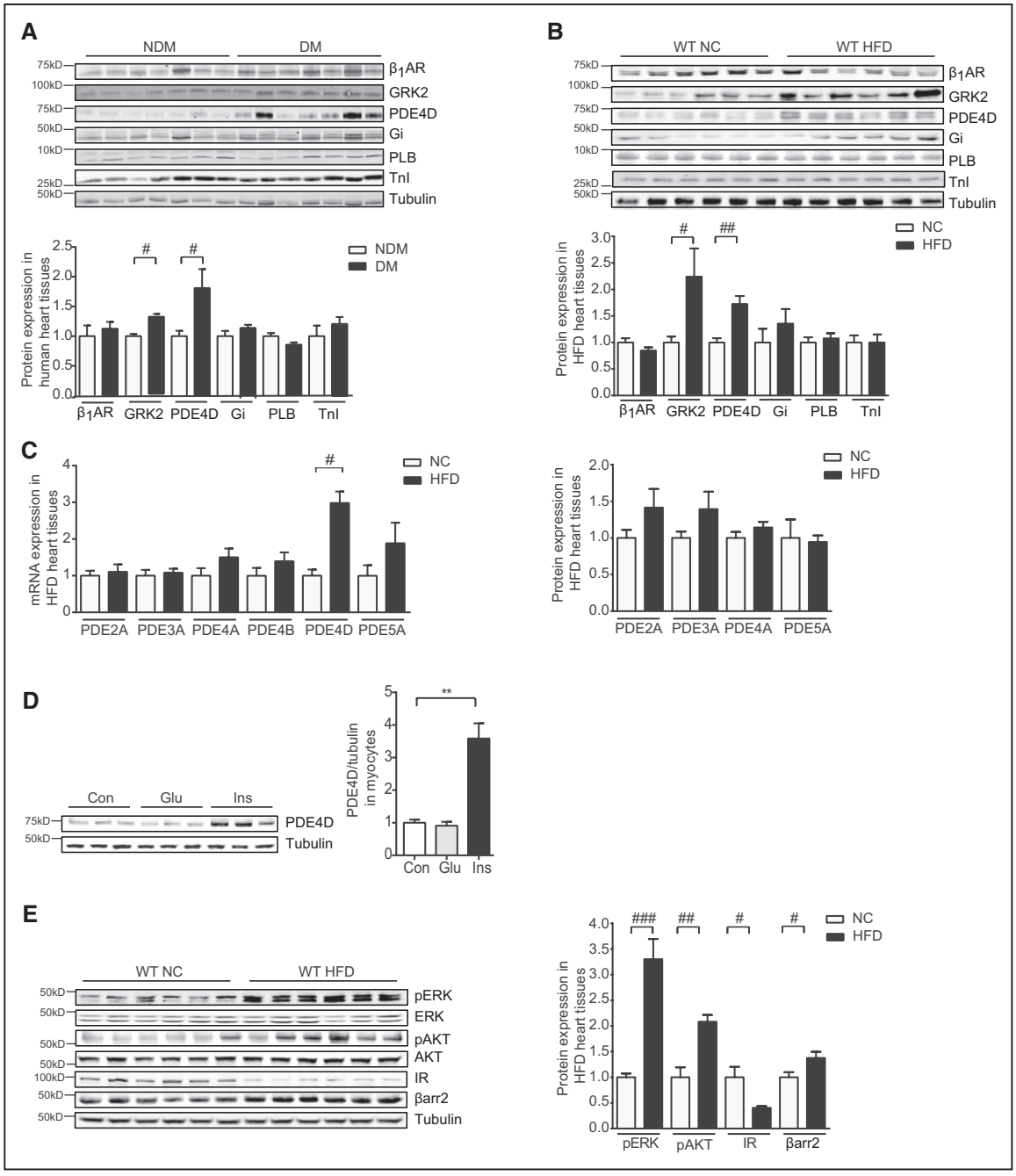

Figure 1. Myocardial phosphodiesterase 4D (PDE4D) expression is increased in insulin-resistant states.
A, Right atrial appendage tissues from patients with diabetes mellitus display increased phosphodiesterase 4D (PDE4D) protein levels relative to patients without diabetes mellitus (n=6). **B** and **C**, Six months of high-fat diet (HFD) increases protein and mRNA levels of PDE4D in mouse hearts (n=12). **D**, Overnight treatment with insulin (100 nmol/L) but not glucose (400 mg/dL) increases PDE4D expression levels in mouse adult ventricle myocytes (AVMs) (n=6). $^{**}P<0.01$ by 1-way analysis of variance followed by post hoc Tukey's test. (E) HFD induces activation of extracellular regulated protein kinase (ERK) (T202/Y204) and Akt (S473) despite a decrease in insulin receptor (IR) expression (n=12; $^{\#}P<0.05$, $^{\#\#}P<0.01$, and $^{\#\#\#}P<0.001$ by student *t* test between paired groups). AKT indicates protein kinase B; β_1AR, β1 adrenergic receptor; βarr2, β arrestin 2; Con, control; DM, diabetes mellitus; GI, inhibitory G protein; Glu, glucose; GRK2, G protein-coupled receptor kinase 2; HFD, high fat diet; Ins, insulin; IR, insulin receptor; NC, normal chow; NDM, non-diabetes mellitus; pERK, phosphorylated extracellular signal-regulated kinase; PLB, phospholamban; TnI, troponin I; and WT, wild type.

involved in cardiac contractility were reduced (Figure 2A and 2B). As a consequence, HFD mice developed time-dependent diastolic and systolic cardiac dysfunction (Figure 2C and online-only Data Supplement Table I). In addition, HFD mice displayed reduced PKA phosphorylation of PLB and cardiac reserve in response to β-adrenergic stimulation (Figure 2D and 2E). Taken together, these data link hyperinsulinemia with PDE4D induction, im-

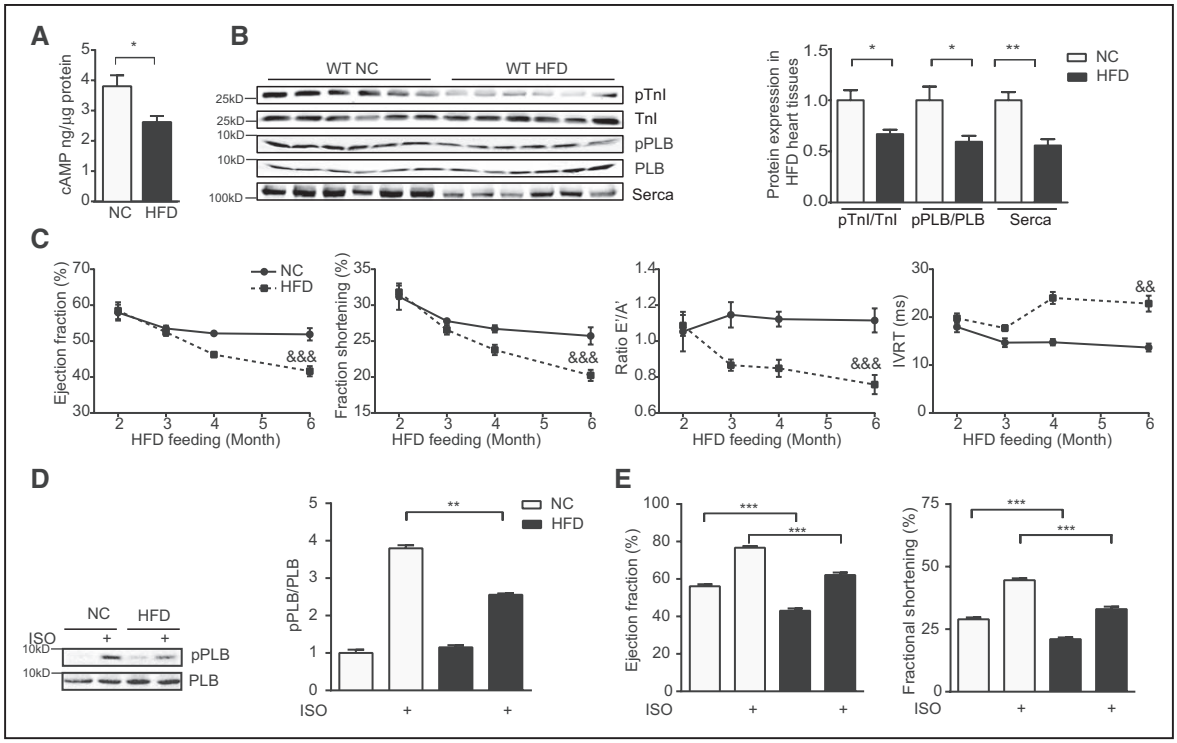

Figure 2. High-fat diet (HFD) impairs adrenergic reserve and induces diastolic and systolic dysfunction in murine hearts. A and **B**, HFD leads to reduced cAMP and protein kinase A (PKA) phosphorylation at serine 16 of phospholamban (PLB) and at serine 23/24 of troponin I (TnI) in mouse hearts. HFD also leads to reduced serca expression (n=12; $^{*}P<0.05$ and $^{**}P<0.01$ by Student's *t* test). **C**, HFD promotes time-dependent systolic and diastolic dysfunction in mouse hearts (n=12; $^{\&\&}P<0.01$ and $^{\&\&\&}P<0.001$ by repeated measures analysis of variance (ANOVA). **D** and **E**, After 6 month of HFD, mouse hearts display reduced PKA phosphorylation of PLB (S16, n=6) and contractile response to β-adrenergic stimulation (ISO, 0.2 mg/kg in vivo, n=12; $^{**}P<0.01$ and $^{***}P<0.001$ by 1-way ANOVA followed by post hoc Tukey's test). cAMP indicates cyclic adenosine monophosphate; E'/A', the ratio of the early (E) to late (A) ventricular filling velocities; HFD, high fat diet; ISO, isoproterenol; IVRT, isovolumic relaxation time; NC, normal chow; PLB, phospholamban; pPLB, phosphorylated phospholamban; pTnI, phosphorylated troponin I; TnI, troponin I; and WT, wild type.

paired inotropic signaling to adrenergic stimulation, and diastolic and systolic dysfunction in murine hearts.

We therefore hypothesized that increased cAMP degradation resulting from increased PDE4D expression in HFD hearts will impair cardiac contractile function in response to adrenergic stimulation. In isolated naïve AVMs, 12-hour incubation with insulin significantly reduced adrenergic (isoproterenol)-induced cAMP levels, which was rescued by a specific PDE4 inhibitor rolipram (Figure 3A). In AVMs isolated from HFD hearts, PKA phosphorylation of both PLB and troponin I in response to adrenergic stimulation was significantly impaired relative to those from NC controls (Figure 3B). In parallel, calcium transients and contractile shortening in response to adrenergic stimulation were also impaired in AVMs from HFD hearts (Figure 3C). The PDE4 inhibitor Rolipram rescued PKA phosphorylation of PLB, calcium transients, and contractile shortening in HFD myocytes (Figure 3B and 3C). These data suggest that hyperinsulinemia-induced PDE4D expression contributes to impaired inotropic signaling in cardiomyocytes.

IR activation promotes 2 major signaling cascades that modulate cellular responses, namely, ERK and Akt. Both ERK and Akt phosphorylation were elevated in HFD hearts. We examined which signaling branch is involved in the induction of PDE4D expression. In isolated AVMs, inhibition of ERK but not Akt completely blocked insulin-induced induction of PDE4D (Figure 4A). We then sought to map the signaling nodes required for ERK activation and PDE4D induction in HFD hearts with strategies in vivo and in cultured cardiomyocytes. We first examined PDE4D expression in the hearts of mice with cardiomyocyte-restricted deletion of IR.[25] As shown in Figure 4B, PDE4D expression was reduced by 50% in cardiomyocyte-restricted deletion of IR mice fed a NC diet and remained repressed after HFD (Figure 4B and 4C). Inhibition of IRS but not GRB2 significantly blocked insulin-induced ERK activation and PDE4D induction in isolated AVMs (Figure 4D and 4E). These data suggest that in this experimental context, ERK activity induced by insulin might be independent of the classical IRS growth factor receptor-bound protein 2 (GRB2)-SOS cascade.

To further explore the underlying mechanisms by which insulin induces PDE4D, we examined the recently characterized membrane IR-β_2AR complex, by which

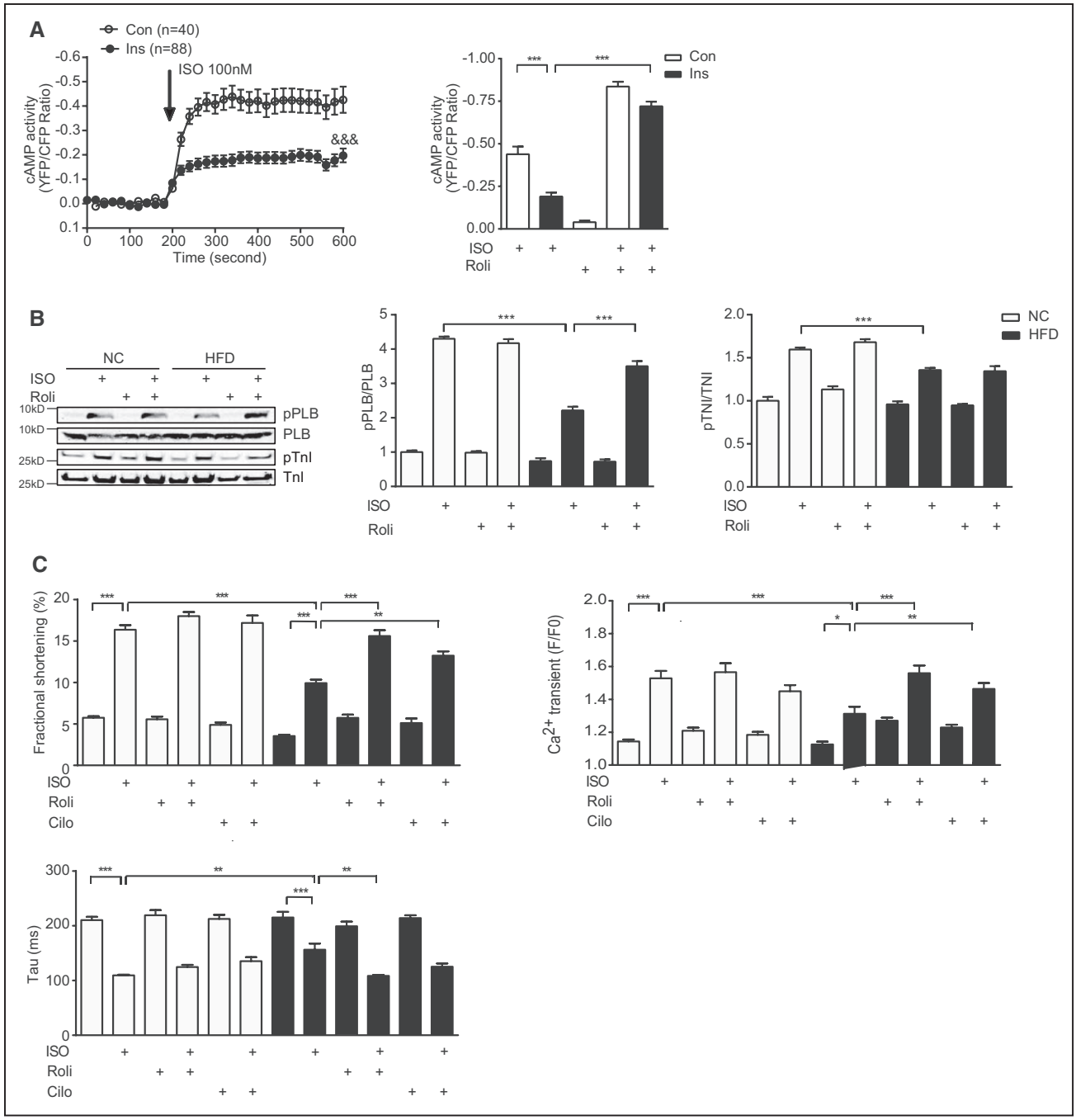

Figure 3. Impaired adrenergic stimulation of cardiac function in hyperinsulinemic states is mediated in part by increased phosphodiesterase 4D (PDE4D) expression.

A, Insulin treatment (100 nmol/L, 12 hrs) impairs adrenergic stimulation of cAMP in mouse adult ventricle myocytes (AVMs), which is rescued by pretreating cells with the PDE4-specific inhibitor rolipram (100 nmol/L, n=6; $^{\&\&\&}P<0.001$ by 2-way analysis of variance [ANOVA], $^{*}P<0.05$, $^{**}P<0.01$, and $^{***}P<0.001$ by 1-way ANOVA followed by post hoc Tukey's test). **B** and **C**, HFD leads to reduced protein kinase A (PKA) phosphorylation of phospholamban (PLB) (S16) and troponin I (TnI) (S23/24), calcium signaling, and contractility in mouse AVMs in response to β-adrenergic stimulation (ISO, 100 nmol/L for AVM stimulation, n=6), which are rescued by the PDE4 inhibitor rolipram (100 nmol/L; $^{**}P<0.01$ and $^{***}P<0.001$ by 1-way ANOVA followed by post hoc Tukey's test). cAMP indicates cyclic adenosine monophosphate; CFP, cyan fluorescent protein; Cilo, cilostamide; Con, control; HFD, high fat diet; Ins, insulin; ISO, isoproterenol; NC, normal chow; PLB, phospholamban; pPLB, phosphorylated phospholamban; pTnI, phosphorylated troponin I; Roli, rolipram; TnI, troponin I; and YFP, yellow fluorescent protein.

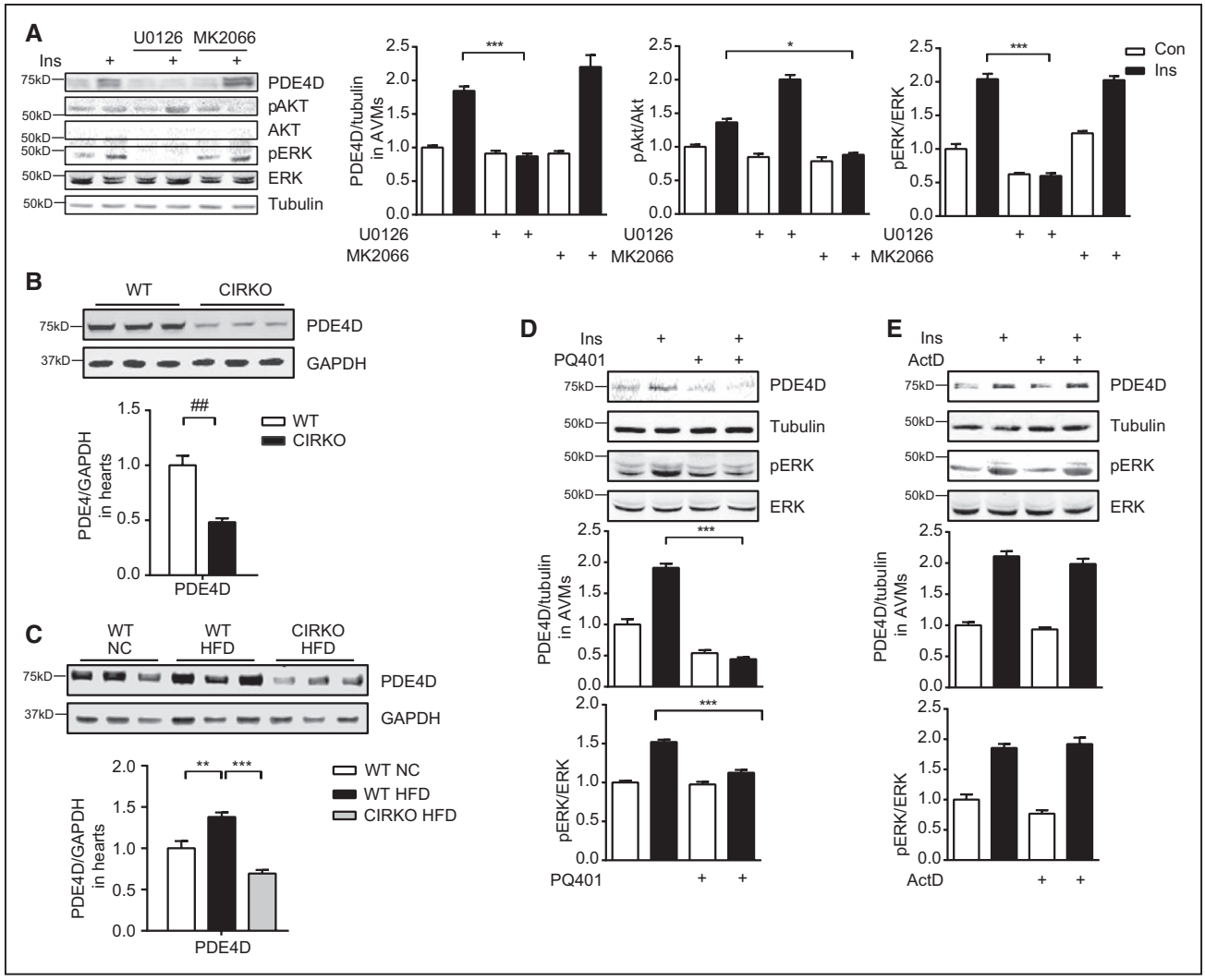

Figure 4. Insulin induces phosphodiesterase 4D (PDE4D) expression in an insulin receptor (IR)- and IR substrate (IRS) dependent manner.

A, Insulin (100 nmol/L) induces PDE4D expression in mouse adult ventricle myocytes (AVMs) that is dependent on extracellular regulated protein kinase (ERK) (T202/Y204) but not Akt (S473) signaling (n=3). **B** and **C**, Decreased PDE4D content in the hearts of mice with cardiomyocyte-restricted deletion of IR (CIRKO) on normal chow or after 36 weeks of a 45% high-fat diet (HFD) (n=6). **D** and **E**, Insulin-induced ERK activation and PDE4D expression in mouse AVMs is IRS-dependent but growth factor receptor-bound protein 2 (GRB2)-independent (n=3). PQ401 is an IRS inhibitor, and actinomycin D (ActD) is an inhibitor of GRB2 (*P<0.05, **P<0.01, and ***P<0.001 by 1-way analysis of variance [ANOVA] followed by post hoc Tukey's test). ActD indicates actinomyosin D; AKT, protein kinase B; AVMs, adult ventricle myocytes; CIRKO, cardiac insulin receptor knockout; Con, control; ERK, extracellular signal-regulated kinase; GAPDH, Glyceraldehyde 3-phosphate dehydrogenase; HFD, high fat diet; Ins, insulin; NC, normal chow; pERK, phosphorylated extracellular signal-regulated kinase; and WT, wild type.

stimulation of the IR leads to an IRS-dependent and GRK2-mediated phosphorylation of the β_2AR.[17,32] We hypothesized that the insulin-induced and GRK2-phosphorylated β_2AR might promote arrestin-dependent ERK activation.[35] Indeed, β_2AR formed a complex with β-arr2 and ERK in cardiac myocytes after insulin stimulation; the receptor-bound ERK displayed increased activity (online-only Data Supplement Figure IIIA). Deletion of either β_2AR or β-arr2 almost completely blocked insulin-induced ERK activation and PDE4D induction (Figure 5A and 5B). In contrast, deletion of β_1AR did not affect insulin-induced ERK activation and PDE4D induction (online-only Data Supplement Figure IIIB). Meanwhile, a clinical nonselective β-blocker carvedilol with arrestin-biased properties and a neutral nonselective β-blocker timolol both attenuated insulin-induced ERK activation and PDE4D induction (online-only Data Supplement Figure IIIC). Moreover, in β_2AR-KO AVMs, reintroduction of wild-type but not mutant β_2AR lacking the GRK phosphorylation sites restored insulin-induced ERK activation and PDE4D induction (Figure 5C). Furthermore, a selective serotonin reuptake inhibitor, paroxetine, which also acts as a specific GRK2 inhibitor,[36]

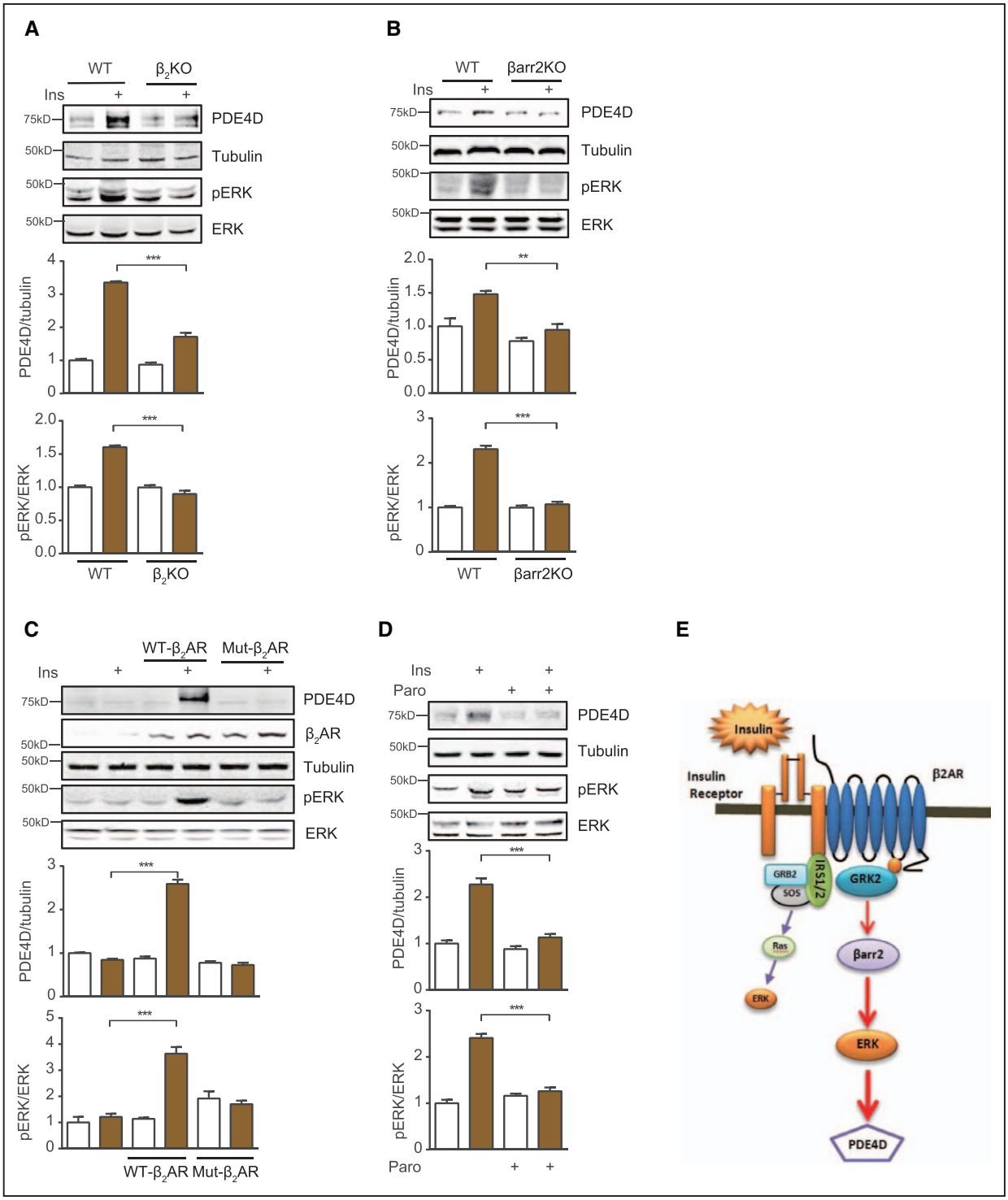

Figure 5. Insulin promotes phosphodiesterase 4D (PDE4D) expression by transactivation of a β_2-adrenergic receptor (β_2AR)-β-arrestin2 (β-arr2)-ERK signaling cascade.

A and **B**, Insulin-induced ERK activation and PDE4D expression in mouse adult ventricle myocytes (AVMs) is dependent on β_2AR and β-arr2 (n=3). **C**, In β_2AR knockout AVMs, reintroduction of wild-type but not β_2AR-GRKmut lacking serine 355/356 rescues insulin-induced ERK activation and PDE4D expression (n=3). **D**, Insulin-induced ERK activation (T202/Y204) and PDE4D expression in mouse AVMs is blocked by a GRK2 inhibitor paroxetine (Paro, 100μM; n=3). **E**, Cartoon depicts the signaling intermediates involved in insulin-induced ERK activation and PDE4D expression (**P<0.01 and ***P<0.001 by 1-way analysis of variance [ANOVA] followed by post hoc Tukey's test). β_2AR indicates β2 adrenergic receptor; β_2KO, β2 adrenergic receptor knockout; βarr2, β arrestin 2; ERK, extracellular signal-regulated kinase; Ins, insulin; IRS1/2, insulin receptor substrate 1/2; Mut-β_2AR, mutant β2 adrenergic receptor; Paro, paroxetine; pERK, phosphorylated extracellular signal-regulated kinase; SOS, son of seven less; and WT, wild type.

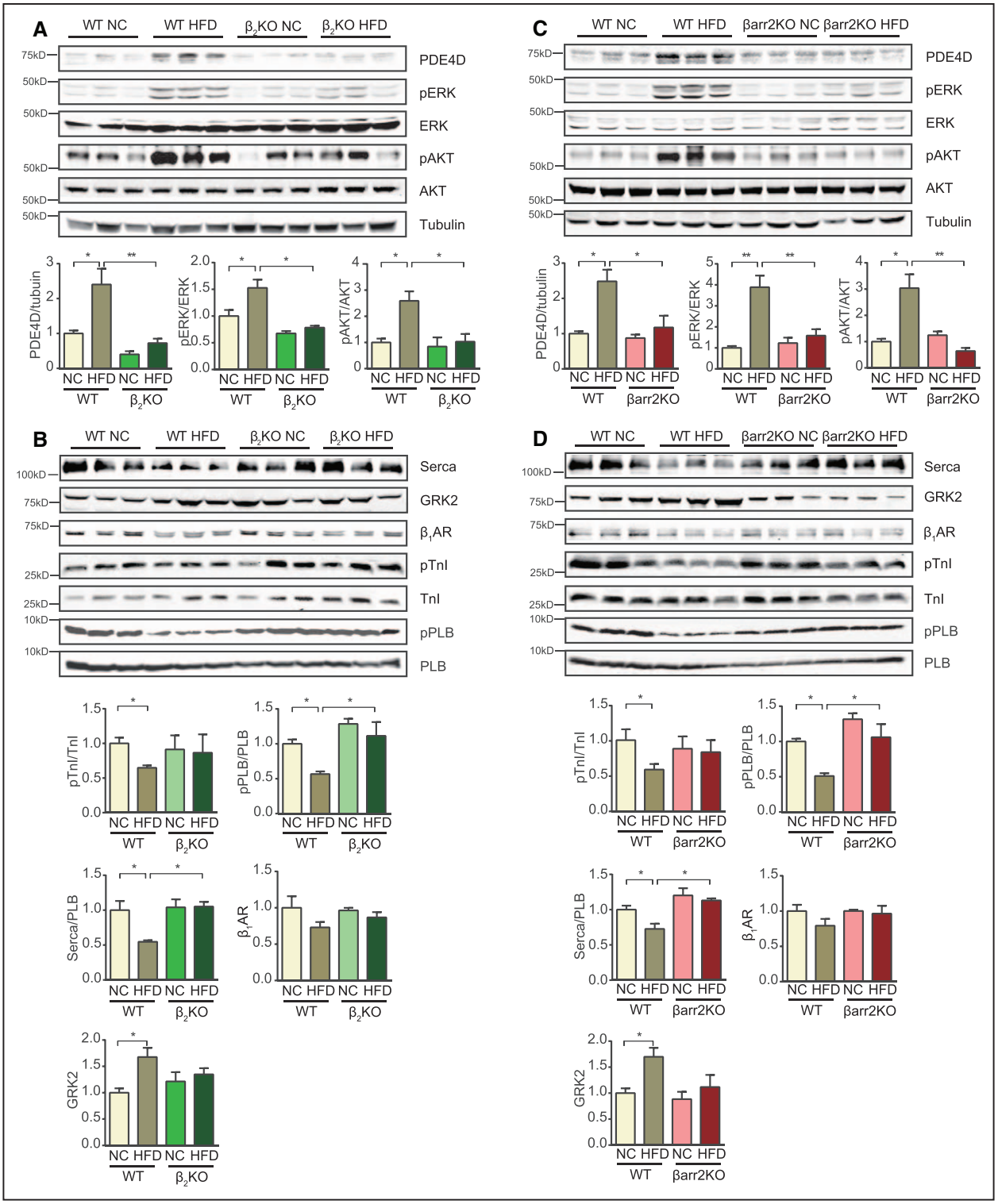

Figure 6. Deletion of β_2-adrenergic receptor (β_2AR) and β-arrestin2 (β-arr2) prevents phosphodiesterase 4D (PDE4D) induction in hearts of high-fat diet (HFD) mice.

A, Deletion of β_2AR prevented HFD-induced activation of extracellular regulated protein kinase (ERK) (T202/Y204) and Akt (S473) and PDE4D induction in mouse hearts (n=12). **B**, Deletion of β_2AR normalizes protein kinase A (PKA) phosphorylation of phospholamban (PLB) (S16) and troponin I (TnI) (S23/24), the ratio of serca2/PLB in mouse hearts and attenuates the induction of growth factor receptor-bound protein 2 (GRK2) (n=12). **C**, Deletion of β-arr2 prevents HFD-induced activation of ERK and Akt and PDE4D induction in mouse hearts (n=12). **D**, Deletion of β-arr2 normalizes PKA phosphorylation of PLB (S16) and TnI (S23/24), the ratio of serca2/PLB in mouse hearts, and prevents the induction of GRK2 (n=12; $*P<0.05$ and $**P<0.01$ by 1-way analysis of variance [ANOVA] followed by post hoc Tukey's test). AKT indicates protein kinase B; β1AR, β1 adrenergic (*Continued*)

significantly blocked insulin-induced ERK activation and PDE4D induction (Figure 5D), whereas another selective serotonin reuptake inhibitor, fluoxetine, did not affect insulin-induced ERK activation and PDE4D induction (online-only Data Supplement Figure 3D). These data support the existence of a novel IR/IRS-induced and GRK-mediated transactivation of a β_2AR-β-arr2-ERK signaling cascade, which is the primary mediator of insulin-induced ERK activation in cardiomyocytes and is also necessary for insulin-induction of PDE4D expression (Figure 5E).

To determine whether this novel IR signaling cascade impairs the activation of signaling mediators of excitation-contraction (EC) coupling and contributes to cardiac dysfunction associated with DM, mice with germline deletion of either β_2AR or β-arr2 gene were fed with HFD or NC. On the HFD, these mutant mice still became obese and diabetic (online-only Data Supplement Figure IVA through IVD) and developed cardiac hypertrophy, but myocardial fibrosis and apoptosis were prevented (online-only Data Supplement Figure VA through VD and Table II). Deletion of these genes blocked activation of ERK and Akt phosphorylation and PDE4D induction in HFD hearts (Figure 6A and 6C and online-only Data Supplement Figure VIA and VIB). Deletion of either gene normalized PKA phosphorylation of PLB and troponin I (Figure 6B and 6D). Deletion of either gene also normalized the ratio of serca2 to PLB, which was reduced in wild-type HFD hearts (Figure 6B and 6D). Accordingly, deletion of either gene blocked the decrease in cAMP levels in HFD hearts (Figure 7A). Moreover, deletion of either β_2AR or β-arr2 genes significantly ameliorated cardiac dysfunction induced by HFD feeding (Figure 7B). In AVMs from HFD hearts lacking the β_2AR or β-arr2 gene, calcium transients and contractile shortening in response to adrenergic stimulation were normal relative to those from NC hearts (Figure 7C and 7D). The PDE4 inhibitor rolipram did not further enhance calcium transients and contractile shortening in HFD myocytes (Figure 7C and 7D). These data suggest that deletion of either β_2AR or β-arr2 significantly restored contractility in cardiomyocytes and ameliorated cardiac dysfunction in hearts.

This novel IR-induced transactivation of the β_2AR-β-arr2-ERK signaling module presents new therapeutic opportunities to treat/prevent cardiac dysfunction associated with DM. We therefore tested whether blocking GRK2-mediated transactivation of the β_2AR would be effective in attenuating cardiac dysfunction induced by HFD. Animals fed with HFD for 4 months displayed cardiac dysfunction (Figure 2C); mice were then subjected to 1-month therapy with vehicle, the GRK2-specific inhibitor paroxetine that was recently shown to be effective in treating myocardial infarction-induced heart failure,[37] or carvedilol, the clinically effective nonselective β-blocker that blocks both β_1AR and β_2AR. Both paroxetine and carvedilol treatments attenuated ERK and Akt activities and PDE4D induction in hearts relative to animals treated with vehicle alone, with paroxetine treatment being more effective (Figure 8A). Both treatments normalized cAMP levels and PKA phosphorylation of PLB and troponin I in HFD hearts relative to vehicle-treated mice (Figure 8B and 8C) and normalized the ratio of serca2 and PLB (Figure 8C). Paroxetine and carvedilol did not alter fasting glucose concentrations but partially improved glucose tolerance, although hyperinsulinemia persisted (online-only Data Supplement Figure VIIA and VIIB). Despite modest effects on systemic metabolic homeostasis, cardiac fibrosis and apoptosis were largely reversed in HFD mice, although cardiac hypertrophy persisted (online-only Data Supplement Figure VIIIA through VIIIC). It is important to note that paroxetine and carvedilol significantly improved cardiac dysfunction compared with HFD mice treated with vehicle (Figure 8D and online-only Data Supplement Table III).

DISCUSSION

Hyperinsulinemia is an independent risk factor for ischemic cardiac disease and predicts coronary atherosclerosis.[38,39] Moreover, hyperinsulinemia has been correlated with depressed adrenergic signaling, which may contribute to systolic and diastolic dysfunction in diabetes, despite elevated catecholamine levels, presumably because of either dysfunctional calcium handling within cardiomyocytes or catecholamine-induced βAR down-regulation.[13–16]The present study demonstrates that hyperinsulinemia directly impairs cardiac function by depressing cardiomyocyte adrenergic signaling. We describe a novel mechanism, whereby hyperinsulinemia remodels adrenergic signal transduction pathways by selectively increasing the expression of PDE4D but not of βARs. Hyperinsulinemia drives a novel IR signaling cascade by IRS- and GRK2-dependent transactivation of a β_2AR-arr-ERK pathway to promote expression of the PDE4D gene. The elevated PDE4D enzyme reduces cAMP activity and PKA phosphorylation of its substrates that may contribute to reduced myocyte calcium cycling and contractile shortening, and systolic and diastolic cardiac dysfunction. Pharmacological inhibition of GRK2 or the β_2AR can effectively reverse cardiac dysfunction induced by HFD.

Mechanistically, IR and β_2AR form a membrane complex in cardiomyocytes.[17,32] Activation of IR promotes

Figure 6 Continued. receptor; β_2KO, β2 adrenergic receptor knockout; βarr2, β arrestin 2; ERK, extracellular signal-regulated kinase; GRK2, G protein-coupled receptor kinase 2; HFD, high fat diet; NC, normal chow; pERK, phosphorylated extracellular signal-regulated kinase; PLB, phospholamban; pPLB, phosphorylated phospholamban; pTnI, phosphorylated troponin I; TnI, troponin I; and WT, wild type.

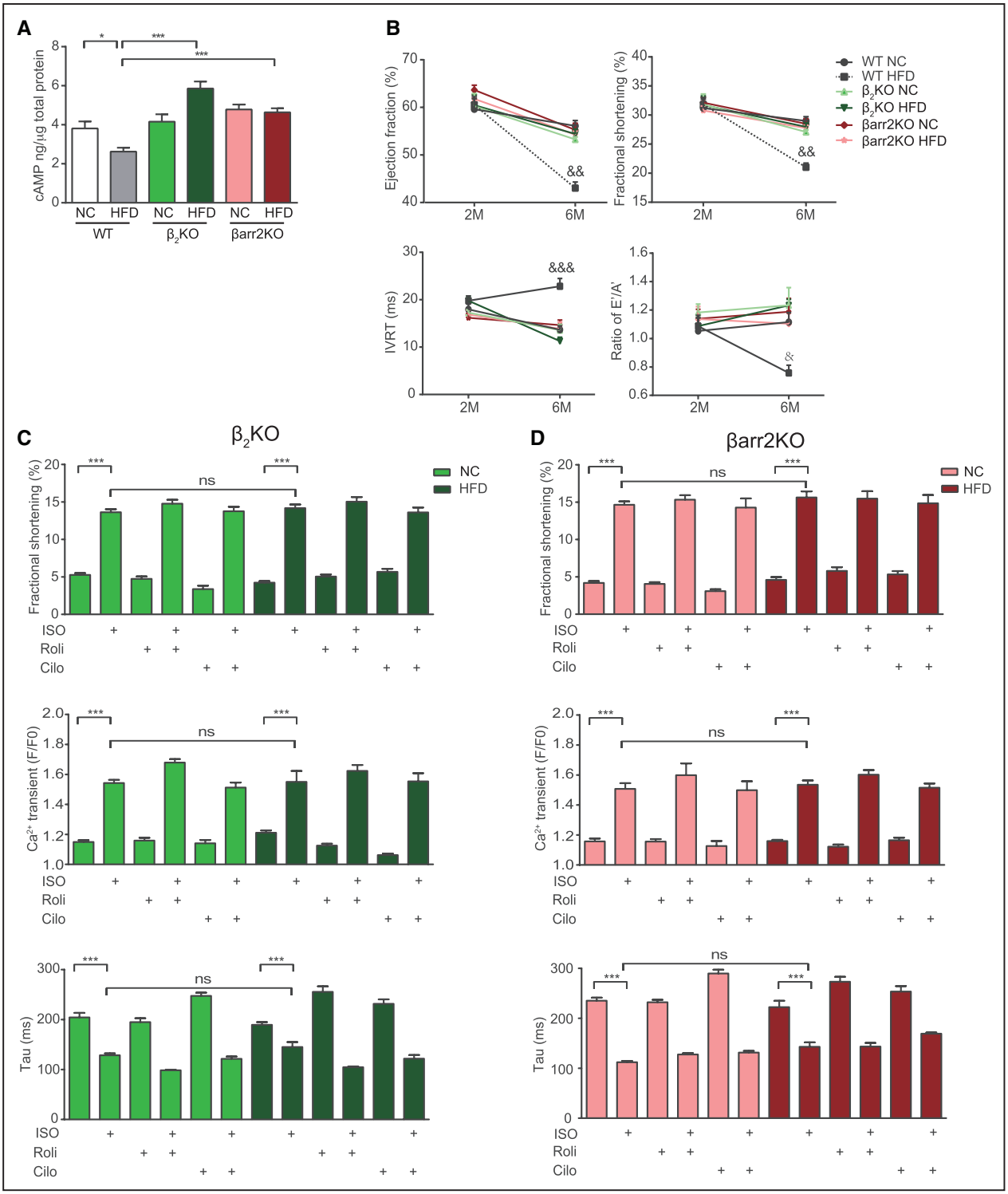

Figure 7. Deletion of β_2-adrenergic receptor (β_2AR) and β-arrestin2 (β-arr2) ameliorates cardiac dysfunction in high-fat diet (HFD) mice.

A, Deletion of β_2AR or β-arr2 prevents down-regulation of cAMP activity (n=12). **B**, Deletion of β_2AR or β-arr2 ameliorates both systolic and diastolic dysfunction induced by HFD (n=12; $^{\&}P<0.05$, $^{\&\&}P<0.01$, and $^{\&\&\&}P<0.001$ by repeated measures analysis of variance [ANOVA]). **C**, Deletion of β_2AR normalizes calcium signaling and contractile shortening in myocytes after HFD feeding (n=4). **D**, Deletion of β-arr2 normalizes calcium signaling and contractile shortening in myocytes after HFD feeding (n=4; $^{*}P<0.05$ and $^{***}P<0.001$ by 1-way ANOVA followed by post hoc Tukey's test). β_2KO indicates β2 adrenergic receptor knockout; βarr2, β arrestin 2; cAMP, cyclic adenosine monophosphate; Cilo, cilostamide; HFD, high fat diet; ISO, isoproterenol; IVRT, isovolumic relaxation time; NC, normal chow; Roli, rolipram; and WT, wild type.

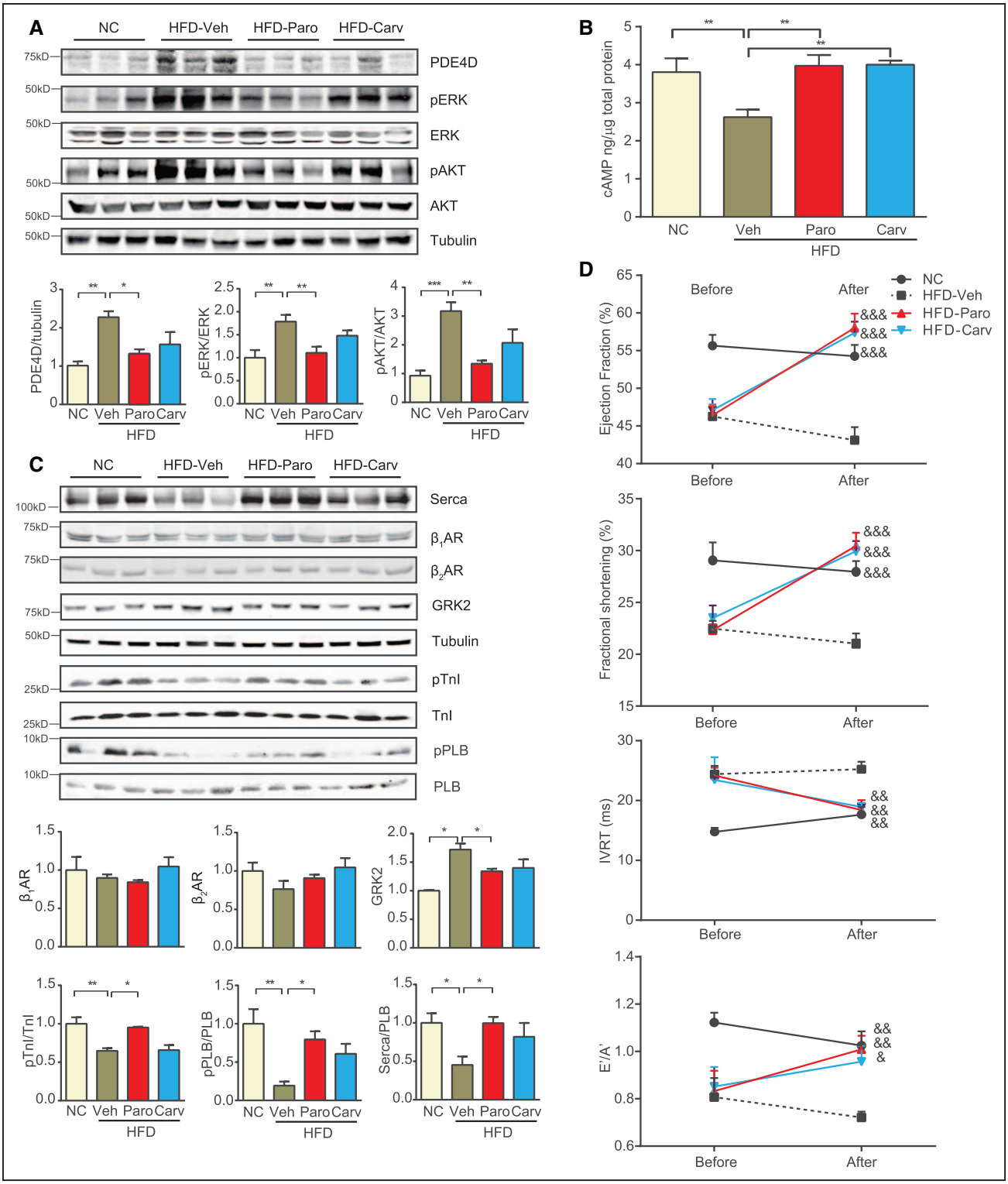

Figure 8. The growth factor receptor-bound protein 2 (GRK2) inhibitor paroxetine and the nonselective β-blocker carvedilol prevent high-fat diet-induced phosphodiesterase 4D (PDE4D) induction and cardiac dysfunction.

A, The GRK2 inhibitor paroxetine (2.5 mg/kg, 1 month) and the β-blocker carvedilol (2.5 mg/kg, 1 month) blocks HFD-induced extracellular regulated protein kinase (ERK) and Akt activation and PDE4D induction in mouse hearts (n=12). **B** and **C**, Paroxetine and carvedilol block HFD-induced reduction of cAMP, protein kinase A (PKA) phosphorylation of phospholamban (PLB) (S16) and troponin I (TnI) (S23/24), the ratio of serca2/PLB, and prevents the induction of GRK2 in mouse hearts (n=12). (D) Paroxetine and carvedilol treatment for 1 month ameliorates cardiac dysfunction in HFD models (n=12; **P*<0.05, (*Continued*)

IRS and GRK2-mediated phosphorylation of the β_2AR,[17,32] which leads to arrestin-dependent ERK activation (Figure 4). Therefore, IR induces arrestin-biased transactivation of the β_2AR in a GRK2 phosphorylation-dependent manner. It is surprising that this new signaling branch is the major mediator of ERK activity induced by insulin, whereas the classic IRS-GRB2-SOS axis appears to play a minor role in promoting insulin-induced ERK activation in the heart (Figure 5). Moreover, our data suggest that only the β_2AR-dependent activation of ERK is necessary for gene expression of PDE4 in cardiomyocytes and hearts, suggesting that insulin signaling may activate distinct pools of ERK, leading to diverse cellular responses. Insulin-induced transactivation of the β_2AR may also play a role in Akt activation, which could promote cardiac hypertrophy independently of the ERK-PDE4D axis. Hyperinsulinemia and hyperglycemia persist in both wild-type and β_2AR-KO hearts after HFD feeding. Despite these metabolic defects, β_2AR-KO myocytes and mice after HFD feeding display normalized contractile shortening and cardiac function, respectively, arguing that the improved cardiac function is largely independent of changes in systemic metabolism but may be caused, in part, by the currently characterized cardiac insulin-β_2AR-arr-ERK pathway that induces PDE4D expression. A recent study shows that genetic ablation of GRK2 is effective in ameliorating adiposity and improving plasma levels of insulin, insulin signaling, and glucose intolerance in a HFD-induced diabetes animal model.[40,41] We also observed attenuation of glucose intolerance in HFD mice after therapy with the GRK2 inhibitor paroxetine (online-only Data Supplement Figure III), although not to the same extent. Thus, global improvement in insulin signaling could also contribute, in part, to the beneficial effects of GRK2 inhibition on cardiac function. Genetic and pharmacological inhibition of the cardiac insulin-β_2AR-arr pathway also attenuates the expression of cardiac GRK2 levels, which may contribute to improved cardiac function. Together these data suggest that adrenergic signaling and metabolic regulation may represent 2 independent therapeutic modalities to prevent or treat heart failure associated with obesity or type 2 DM.

Phosphodiesterases play essential roles in modulating ion channel activity, such as L-type calcium channels, ryanodine receptors and the serca2 pump, which controls EC coupling in cardiomyocytes.[42–47] PDE3 and PDE4 are the major PDEs in both rodent and human hearts.[48] Recent studies indicated that the expression of PDEs is altered in diverse disease models,[49] potentially as an adaptation to early stage disease. In contrast, deletion of the PDE4D gene leads to spontaneous heart failure.[42] These observations suggest that phosphodiesterases play an essential role in maintaining a fine balance of tonic cAMP-PKA activity for tissue integrity and function in hearts. Here we show that in a model of insulin resistance and type 2 DM, activation of insulin-signaling pathways mediates the induction of PDE4D. Although myocytes isolated from mice after HFD feeding display impaired calcium signaling and contractile shortening, inhibition of PDE4 but not PDE3 completely rescued calcium signaling and contractile function after adrenergic stimulation. Taken together with earlier observations indicating hyperactivation of insulin signaling in failing human hearts[9] and the attenuation of heart failure when insulin signaling is reduced in a model of transverse aortic constriction,[7] these observations suggest that insulin-induced induction of PDE4 may be a central mechanism that contributes to heart failure. Further studies are needed to directly assess a role for PDE4 in obesity- and DM-associated cardiac dysfunction in vivo.

A detailed mechanistic understanding of the interactions between hyperinsulinemia and heart failure remains to be achieved. For example, the divergence between fibrosis, which was attenuated by inhibiting β_2AR and GRK2 signaling, despite persistence of cardiac hypertrophy, underlies the complex interactions of these signaling pathways on distinct elements of cardiac remodeling. Thus, mechanisms linking cardiomyocyte ERK activation to the development of cardiac fibrosis in the context of metabolic disorders will be the focus of future investigations. Moreover, we have also previously shown that acute insulin treatment inhibits cardiac contractility by inducing G_i-biased β_2AR signaling in hearts.[17,32] Whether this G_i pathway contributes to insulin-induced transactivation of β_2AR-arr-ERK, leading to cardiac dysfunction, remains to be examined. Furthermore, despite reduced IR levels in HFD hearts, the remaining IRs are still sufficient to activate ERK and Akt signaling in the face of persistent hyperinsulinemia. These signaling changes may lead to defects in cardiac metabolism or structural remodeling, including cardiac fibrosis. Indeed, although the focus of this study is on the relationship between ERK activation and PDE4D induction, which clearly might contribute to decreased cardiac contractility, it is possible that the cardiac fibrosis observed, although dependent on ERK signaling, could be independent of the induction of PDE4D.

These studies have important translational implications given the large number of individuals with the metabolic syndrome and the significant enrichment of heart

Figure 8 Continued. $^{**}P<0.01$, and $^{***}P<0.001$ by 1-way analysis of variance [ANOVA] followed by post hoc Tukey's test; $^{\&}P<0.05$, $^{\&\&}P<0.01$, and $^{\&\&\&}P<0.001$ by repeated measures ANOVA). AKT indicates protein kinase B; B_1AR, β1 adrenergic receptor; B_2AR, β2 adrenergic receptor; Carv, cavedilol; ERK, extracellular signal-regulated kinase; GRK2, G protein-coupled receptor kinase 2; HFD, high fat diet; NC, normal chow; Paro, paroxetine; pERK, phosphorylated extracellular signal-regulated kinase; PLB, phospholamban; pPLB, phosphorylated phospholamban; pTnI, phosphorylated troponin I; TnI, troponin I; and Veh, vehicle.

failure among subjects with DM.[50] Hyperinsulinemia is a cardinal characteristic of patients with heart failure and also of those with the metabolic syndrome and type 2 DM, many of whom require high doses of insulin to achieve metabolic control. Thus, hyperinsulinemia by increasing the expression of PDE4 may exacerbate heart failure by limiting ventricular contractile reserve on the basis of reduced myocardial cAMP/PKA activity. Epidemiological and clinical observations have linked insulin treatment with increased mortality in patients with heart failure with diabetes.[21] Conversely, blocking the IR-induced β_2AR-ERK signaling pathway either genetically or pharmacologically significantly alleviates the cardiac dysfunction (Figures 7 and 8). In agreement, β blockade with either metoprolol[22] or carvedilol[23] reduces mortality in subjects with heart failure with DM, with the possibility that agents possessing β_2 selective inhibition could be somewhat more effective.[24] The present study suggests a specific role for the β_2AR in hyperinsulinemia-induced cardiac dysfunction. Despite its property as an arrestin-biased ligand, carvedilol can attenuate insulin-induced ERK activation and PDE4 induction in vitro and in vivo. It is also possible that the β_1AR could be activated as a consequence of the compensatory elevation of sympathetic drive, thereby indirectly contributing to cardiac dysfunction in hyperinsulinemic states. It remains to be determined whether the β_1AR selective agent metoprolol is effective in ameliorating cardiac systolic and diastolic dysfunction. Paroxetine is an FDA-approved selective serotonin reuptake inhibitor that also inhibits GRK2.[36] Paroxetine was recently shown to be effective in treating myocardial infarction-induced heart failure, whereas another selective serotonin reuptake inhibitor, fluoxetine, did not.[37] Our data show that inhibition of GRK2 with paroxetine can also be effective in ameliorating cardiac dysfunction in HFD mice. Thus, in addition to providing new insights into the pathophysiology of heart failure in insulin-resistant states, our study provides a strong rationale for targeting β_2AR- and GRK2-mediated signaling as an attractive therapeutic modality to prevent or treat heart failure associated with type 2 DM.

SOURCES OF FUNDING

Drs Abel and Xiang were supported by National Institutes of Health grants HL127764 and HL112413. Dr Xiang was supported by National Institutes of Health grant S10 OD10389, VA Merit grant 01BX002900, and China NSFC grant 81428022. Dr Abel was supported by National Institutes of Health grant DK092065. Dr Wei was supported by China NSFC grants 81330081. Dr Wang was supported by China NSFC grant 81202541. Dr Fu was supported by China NSFC grant 81473212. Drs Abel and Xiang are established investigators of the American Heart Association, and Dr Xiang is a Shanghai Eastern Scholar. Dr Zhang is supported by a postdoctoral fellowship from the American Heart Association.

DISCLOSURES

None.

AFFILIATIONS

From Department of Pharmacology, University of California at Davis (Q.W., Y.L., Q.F., B.X., S.K., R.T., F.B., T.W., Y.K.X); Institute of Clinical Pharmacology, Anhui Medical University, Key Laboratory of Anti-Inflammatory and Immune Medicine, Ministry of Education, Collaborative Innovation Center of Anti-Inflammatory and Immune Medicine, Hefei, China (Q.W, W.W.); Shuguang Hospital, Shanghai University of Traditional Chinese Medicine (Y.L.); Department of Pharmacology, Tongji Medical College, Huazhong University of Science and Technology, Wuhan, China (Q.F.); Department of Medicine, Division of Endocrinology and Metabolism and Fraternal Order of Eagles Diabetes Research Center, University of Iowa, Iowa City (Y.Z., E.D.A.); Department of Pharmacology and Toxicology, East Carolina University, Greenville, NC (E.A.); and VA Northern California Health Care System, Mather (Y.K.X.).

FOOTNOTES

Received February 29, 2016; accepted October 13, 2016.

The online-only Data Supplement is available with this article at http://circ.ahajournals.org/lookup/suppl/doi:10.1161/CIRCULATIONAHA.116.022281/-/DC1.

Circulation is available at http://circ.ahajournals.org.

REFERENCES

1. Gregg EW, Li Y, Wang J, Burrows NR, Ali MK, Rolka D, Williams DE, Geiss L. Changes in diabetes-related complications in the United States, 1990-2010. *N Engl J Med*. 2014;370:1514–1523. doi: 10.1056/NEJMoa1310799.
2. Bugger H, Abel ED. Molecular mechanisms of diabetic cardiomyopathy. *Diabetologia*. 2014;57:660–671.
3. Hayat SA, Patel B, Khattar RS, Malik RA. Diabetic cardiomyopathy: mechanisms, diagnosis and treatment. *Clin Sci (Lond)*. 2004;107:539–557. doi: 10.1042/CS20040057.
4. Boudina S, Abel ED. Diabetic cardiomyopathy revisited. *Circulation*. 2007;115:3213–3223.
5. Abel ED, O'Shea KM, Ramasamy R. Insulin resistance: metabolic mechanisms and consequences in the heart. *Arteriosclerosis, thrombosis, and vascular biology*. 2012;32:2068–2076.
6. Taegtmeyer H, Beauloye C, Harmancey R, Hue L. Insulin resistance protects the heart from fuel overload in dysregulated metabolic states. *Am J Physiol Heart Circ Physiol*. 2013;305:H1693–H1697. doi: 10.1152/ajpheart.00854.2012.
7. Shimizu I, Minamino T, Toko H, Okada S, Ikeda H, Yasuda N, Tateno K, Moriya J, Yokoyama M, Nojima A, Koh GY, Akazawa H, Shiojima I, Kahn CR, Abel ED, Komuro I. Excessive cardiac insulin signaling exacerbates systolic dysfunction induced by pressure overload in rodents. *J Clin Invest*. 2010;120:1506–1514.
8. Wende AR, O'Neill BT, Bugger H, Riehle C, Tuinei J, Buchanan J, Tsushima K, Wang L, Caro P, Guo A, Sloan C, Kim BJ, Wang X, Pereira RO, McCrory MA, Nye BG, Benavides GA, Darley-Usmar VM, Shioi T, Weimer BC, Abel ED. Enhanced cardiac Akt/protein kinase B signaling contributes to pathological cardiac hypertrophy in part by impairing mitochondrial function via transcriptional re-

pression of mitochondrion-targeted nuclear genes. *Molecular and cellular biology*. 2015;35:831–846.
9. Cook SA, Varela-Carver A, Mongillo M, Kleinert C, Khan MT, Leccisotti L, Strickland N, Matsui T, Das S, Rosenzweig A, Punjabi P, Camici PG. Abnormal myocardial insulin signalling in type 2 diabetes and left-ventricular dysfunction. *Eur Heart J*. 2010;31:100–111. doi: 10.1093/eurheartj/ehp396.
10. Battiprolu PK, Hojayev B, Jiang N, Wang ZV, Luo X, Iglewski M, Shelton JM, Gerard RD, Rothermel BA, Gillette TG, Lavandero S, Hill JA. Metabolic stress-induced activation of FoxO1 triggers diabetic cardiomyopathy in mice. *J Clin Invest*. 2012;122:1109–1118. doi: 10.1172/JCI60329.
11. Qi Y, Zhu Q, Zhang K, Thomas C, Wu Y, Kumar R, Baker KM, Xu Z, Chen S, Guo S. Activation of Foxo1 by insulin resistance promotes cardiac dysfunction and β-myosin heavy chain gene expression. *Circ Heart Fail*. 2015;8:198–208. doi: 10.1161/CIRCHEARTFAILURE.114.001457.
12. Qi Y, Xu Z, Zhu Q, Thomas C, Kumar R, Feng H, Dostal DE, White MF, Baker KM, Guo S. Myocardial loss of IRS1 and IRS2 causes heart failure and is controlled by p38α MAPK during insulin resistance. *Diabetes*. 2013;62:3887–3900. doi: 10.2337/db13-0095.
13. Bell DS. Heart failure: the frequent, forgotten, and often fatal complication of diabetes. *Diabetes Care*. 2003;26:2433–2441.
14. Ganguly PK, Pierce GN, Dhalla KS, Dhalla NS. Defective sarcoplasmic reticular calcium transport in diabetic cardiomyopathy. *Am J Physiol*. 1983;244:E528–E535.
15. Giacomelli F, Wiener J. Primary myocardial disease in the diabetic mouse: an ultrastructural study. *Lab Invest*. 1979;40:460–473.
16. Bell DS. Diabetic cardiomyopathy: a unique entity or a complication of coronary artery disease? *Diabetes Care*. 1995;18:708–714.
17. Fu Q, Xu B, Liu Y, Parikh D, Li J, Li Y, Zhang Y, Riehle C, Zhu Y, Rawlings T, Shi Q, Clark RB, Chen X, Abel ED, Xiang YK. Insulin inhibits cardiac contractility by inducing a Gi-biased beta2-adrenergic signaling in hearts. *Diabetes*. 2014;63:2676–2689.
18. Nichols GA, Hillier TA, Erbey JR, Brown JB. Congestive heart failure in type 2 diabetes: prevalence, incidence, and risk factors. *Diabetes Care*. 2001;24:1614–1619.
19. Castagno D, Baird-Gunning J, Jhund PS, Biondi-Zoccai G, MacDonald MR, Petrie MC, Gaita F, McMurray JJ. Intensive glycemic control has no impact on the risk of heart failure in type 2 diabetic patients: evidence from a 37 229 patient meta-analysis. *Am Heart J*. 2011;162:938.e2–948.e2. doi: 10.1016/j.ahj.2011.07.030.
20. Scirica BM, Braunwald E, Raz I, Cavender MA, Morrow DA, Jarolim P, Udell JA, Mosenzon O, Im K, Umez-Eronini AA, Pollack PS, Hirshberg B, Frederich R, Lewis BS, McGuire DK, Davidson J, Steg PG, Bhatt DL; SAVOR-TIMI 53 Steering Committee and Investigators*. Heart failure, saxagliptin, and diabetes mellitus: observations from the SAVOR-TIMI 53 randomized trial. *Circulation*. 2014;130:1579–1588. doi: 10.1161/CIRCULATIONAHA.114.010389.
21. Smooke S, Horwich TB, Fonarow GC. Insulin-treated diabetes is associated with a marked increase in mortality in patients with advanced heart failure. *Am Heart J*. 2005;149:168–174. doi: 10.1016/j.ahj.2004.07.005.
22. Deedwania PC, Giles TD, Klibaner M, Ghali JK, Herlitz J, Hildebrandt P, Kjekshus J, Spinar J, Vitovec J, Stanbrook H, Wikstrand J; MERIT-HF Study Group. Efficacy, safety and tolerability of metoprolol CR/XL in patients with diabetes and chronic heart failure: experiences from MERIT-HF. *Am Heart J*. 2005;149:159–167. doi: 10.1016/j.ahj.2004.05.056.
23. Bell DS, Lukas MA, Holdbrook FK, Fowler MB. The effect of carvedilol on mortality risk in heart failure patients with diabetes: results of a meta-analysis. *Curr Med Res Opin*. 2006;22:287–296. doi: 10.1185/030079906X80459.
24. Torp-Pedersen C, Metra M, Charlesworth A, Spark P, Lukas MA, Poole-Wilson PA, Swedberg K, Cleland JG, Di Lenarda A, Remme WJ, Scherhag A; COMET investigators. Effects of metoprolol and carvedilol on pre-existing and new onset diabetes in patients with chronic heart failure: data from the Carvedilol or Metoprolol European Trial (COMET). *Heart*. 2007;93:968–973. doi: 10.1136/hrt.2006.092379.
25. Belke DD, Betuing S, Tuttle MJ, Graveleau C, Young ME, Pham M, Zhang D, Cooksey RC, McClain DA, Litwin SE, Taegtmeyer H, Severson D, Kahn CR, Abel ED. Insulin signaling coordinately regulates cardiac size, metabolism, and contractile protein isoform expression. *J Clin Invest*. 2002;109:629–639.
26. Shiojima I, Yefremashvili M, Luo Z, Kureishi Y, Takahashi A, Tao J, Rosenzweig A, Kahn CR, Abel ED, Walsh K. Akt signaling mediates postnatal heart growth in response to insulin and nutritional status. *J Biol Chem*. 2002;277:37670–37677.
27. Laustsen PG, Russell SJ, Cui L, Entingh-Pearsall A, Holzenberger M, Liao R, Kahn CR. Essential role of insulin and insulin-like growth factor 1 receptor signaling in cardiac development and function. *Mol Cell Biol*. 2007;27:1649–1664. doi: 10.1128/MCB.01110-06.
28. Xiang Y, Kobilka BK. Myocyte adrenoceptor signaling pathways. *Science*. 2003;300:1530–1532. doi: 10.1126/science.1079206.
29. Xiao RP, Zhu W, Zheng M, Cao C, Zhang Y, Lakatta EG, Han Q. Subtype-specific alpha1- and beta-adrenoceptor signaling in the heart. *Trends Pharmacol Sci*. 2006;27:330–337. doi: 10.1016/j.tips.2006.04.009.
30. Perrino C, Rockman HA. Reversal of cardiac remodeling by modulation of adrenergic receptors: a new frontier in heart failure. *Curr Opin Cardiol*. 2007;22:443–449. doi: 10.1097/HCO.0b013e3282294d72.
31. Brittsan AG, Kranias EG. Phospholamban and cardiac contractile function. *J Mol Cell Cardiol*. 2000;32:2131–2139. doi: 10.1006/jmcc.2000.1270.
32. Fu Q, Xu B, Parikh D, Cervantes D, Xiang YK. Insulin induces IRS2-dependent and GRK2-mediated β2AR internalization to attenuate βAR signaling in cardiomyocytes. *Cell Signal*. 2015;27:707–715. doi: 10.1016/j.cellsig.2014.11.018.
33. Xiang Y, Naro F, Zoudilova M, Jin SL, Conti M, Kobilka B. Phosphodiesterase 4D is required for beta2 adrenoceptor subtype-specific signaling in cardiac myocytes. *Proc Natl Acad Sci U S A*. 2005;102:909–914. doi: 10.1073/pnas.0405263102.
34. Richter W, Day P, Agrawal R, Bruss MD, Granier S, Wang YL, Rasmussen SG, Horner K, Wang P, Lei T, Patterson AJ, Kobilka B, Conti M. Signaling from beta1- and beta2-adrenergic receptors is defined by differential interactions with PDE4. *EMBO J*. 2008;27:384–393. doi: 10.1038/sj.emboj.7601968.
35. Lin FT, Miller WE, Luttrell LM, Lefkowitz RJ. Feedback regulation of beta-arrestin1 function by extracellular signal-regulated kinases. *J Biol Chem*. 1999;274:15971–15974.
36. Thal DM, Homan KT, Chen J, Wu EK, Hinkle PM, Huang ZM, Chuprun JK, Song J, Gao E, Cheung JY, Sklar LA, Koch WJ, Tesmer JJ. Paroxetine is a direct inhibitor of g protein-coupled receptor kinase 2 and increases myocardial contractility. *ACS Chem Biol*. 2012;7:1830–1839. doi: 10.1021/cb3003013.
37. Schumacher SM, Gao E, Zhu W, Chen X, Chuprun JK, Feldman AM, Tesmer JJ, Koch WJ. Paroxetine-mediated GRK2 inhibition reverses cardiac dysfunction and remodeling after myocardial infarction. *Sci Transl Med*. 2015;7:277ra31. doi: 10.1126/scitranslmed.aaa0154.
38. Després JP, Lamarche B, Mauriège P, Cantin B, Lupien PJ, Dagenais GR. Risk factors for ischaemic heart disease: is it time to measure insulin? *Eur Heart J*. 1996;17:1453–1454.
39. Pyörälä M, Miettinen H, Laakso M, Pyörälä K. Hyperinsulinemia predicts coronary heart disease risk in healthy middle-aged men: the 22-year follow-up results of the Helsinki Policemen Study. *Circulation*. 1998;98:398–404.
40. Garcia-Guerra L, Nieto-Vazquez I, Vila-Bedmar R, Jurado-Pueyo M, Zalba G, Díez J, Murga C, Fernández-Veledo S, Mayor F Jr, Lorenzo M. G protein-coupled receptor kinase 2 plays a relevant role

in insulin resistance and obesity. *Diabetes*. 2010;59:2407–2417. doi: 10.2337/db10-0771.
41. Vila-Bedmar R, Cruces-Sande M, Lucas E, Willemen HL, Heijnen CJ, Kavelaars A, Mayor F Jr, Murga C. Reversal of diet-induced obesity and insulin resistance by inducible genetic ablation of GRK2. *Sci Signal*. 2015;8:ra73. doi: 10.1126/scisignal.aaa4374.
42. Lehnart SE, Wehrens XH, Reiken S, Warrier S, Belevych AE, Harvey RD, Richter W, Jin SL, Conti M, Marks AR. Phosphodiesterase 4D deficiency in the ryanodine-receptor complex promotes heart failure and arrhythmias. *Cell*. 2005;123:25–35. doi: 10.1016/j.cell.2005.07.030.
43. Beca S, Helli PB, Simpson JA, Zhao D, Farman GP, Jones PP, Tian X, Wilson LS, Ahmad F, Chen SR, Movsesian MA, Manganiello V, Maurice DH, Conti M, Backx PH. Phosphodiesterase 4D regulates baseline sarcoplasmic reticulum Ca2+ release and cardiac contractility, independently of L-type Ca2+ current. *Circ Res*. 2011;109:1024–1030. doi: 10.1161/CIRCRESAHA.111.250464.
44. Ghigo A, Perino A, Mehel H, Zahradníková A Jr, Morello F, Leroy J, Nikolaev VO, Damilano F, Cimino J, De Luca E, Richter W, Westenbroek R, Catterall WA, Zhang J, Yan C, Conti M, Gomez AM, Vandecasteele G, Hirsch E, Fischmeister R. Phosphoinositide 3-kinase γ protects against catecholamine-induced ventricular arrhythmia through protein kinase A-mediated regulation of distinct phosphodiesterases. *Circulation*. 2012;126:2073–2083. doi: 10.1161/CIRCULATIONAHA.112.114074.
45. Leroy J, Abi-Gerges A, Nikolaev VO, Richter W, Lechêne P, Mazet JL, Conti M, Fischmeister R, Vandecasteele G. Spatiotemporal dynamics of beta-adrenergic cAMP signals and L-type Ca2+ channel regulation in adult rat ventricular myocytes: role of phosphodiesterases. *Circ Res*. 2008;102:1091–1100. doi: 10.1161/CIRCRESAHA.107.167817.
46. Leroy J, Richter W, Mika D, Castro LR, Abi-Gerges A, Xie M, Scheitrum C, Lefebvre F, Schittl J, Mateo P, Westenbroek R, Catterall WA, Charpentier F, Conti M, Fischmeister R, Vandecasteele G. Phosphodiesterase 4B in the cardiac L-type Ca^{2+} channel complex regulates Ca^{2+} current and protects against ventricular arrhythmias in mice. *J Clin Invest*. 2011;121:2651–2661. doi: 10.1172/JCI44747.
47. Timofeyev V, Myers RE, Kim HJ, Woltz RL, Sirish P, Heiserman JP, Li N, Singapuri A, Tang T, Yarov-Yarovoy V, Yamoah EN, Hammond HK, Chiamvimonvat N. Adenylyl cyclase subtype-specific compartmentalization: differential regulation of L-type Ca2+ current in ventricular myocytes. *Circ Res*. 2013;112:1567–1576. doi: 10.1161/CIRCRESAHA.112.300370.
48. Richter W, Xie M, Scheitrum C, Krall J, Movsesian MA, Conti M. Conserved expression and functions of PDE4 in rodent and human heart. *Basic Res Cardiol*. 2011;106:249–262. doi: 10.1007/s00395-010-0138-8.
49. Abi-Gerges A, Richter W, Lefebvre F, Mateo P, Varin A, Heymes C, Samuel JL, Lugnier C, Conti M, Fischmeister R, Vandecasteele G. Decreased expression and activity of cAMP phosphodiesterases in cardiac hypertrophy and its impact on beta-adrenergic cAMP signals. *Circ Res*. 2009;105:784–792. doi: 10.1161/CIRCRESAHA.109.197947.
50. Haas SJ, Vos T, Gilbert RE, Krum H. Are beta-blockers as efficacious in patients with diabetes mellitus as in patients without diabetes mellitus who have chronic heart failure? A meta-analysis of large-scale clinical trials. *Am Heart J*. 2003;146:848–853. doi: 10.1016/S0002-8703(03)00403-4.

Inhibiting Insulin-Mediated β_2-Adrenergic Receptor Activation Prevents Diabetes-Associated Cardiac Dysfunction

Qingtong Wang, Yongming Liu, Qin Fu, Bing Xu, Yuan Zhang, Sungjin Kim, Ruensern Tan, Federica Barbagallo, Toni West, Ethan Anderson, Wei Wei, E. Dale Abel and Yang K. Xiang

Circulation. 2017;135:73-88; originally published online November 4, 2016;
doi: 10.1161/CIRCULATIONAHA.116.022281
Circulation is published by the American Heart Association, 7272 Greenville Avenue, Dallas, TX 75231

Print ISSN: 0009-7322. Online ISSN: 1524-4539

Supplemental Material

Methods

Experimental animals and *in vivo* treatment. The animal care and experimental protocols followed US National Institutes of Health guidelines and were approved by the Institutional Animal Care and Use Committees (IACUC) of the University of California at Davis, the University of Utah and the Carver College of Medicine of the University of Iowa. C57BL/6 mice were purchased from Charles River. Six-week-old male WT, β_2AR global knockout (β_2KO) and β-arrestin2 global knockout (β-arr2 KO) mice randomly assigned to two groups fed ad libitum with either a low-fat diet or a matched high-fat diet (Research Diets Inc.) for six months (n=26). The low fat diet was D12450J (3.85 kcal/g; 10% of calories from fat, 20% of calories from protein and 70% of calories from carbohydrate) and the high fat diet (HFD) was D12492 (5.24 kcal/g; 60% of calories from fat, 20% of calories from protein and 20% of calories from carbohydrate). Blood glucose levels were measured after a fast of 6 hours. Cardiac function was assessed before and after 24 wk. HFD or chow diet by echocardiography under isoflurane anesthesia. Mice were subjected to intraperitoneal glucose tolerance testing (IPGTT) following each echocardiography study. For the treatment experiments, after 14 weeks of HFD feeding, WT mice (n=45) were randomly assigned to three groups according to the cardiac function. Each group were treated by daily oral gavage with vehicle (5% dimethyl sulfoxide (DMSO) in water), paroxetine (2.5 mg/kg in 5% DMSO, Ark Pharm, Libertyville, IL) or carvedilol (2.5mg/kg in 5% DMSO, Cayman Chemical, Ann Arbor, MI) for 4 wk. Metabolic parameters were monitored during the treatment period, including weekly body weight and food consumption and monthly fasting blood glucose levels. Intraperitoneal glucose tolerance tests (IPGTT) and cardiac function were determined prior to and after the respective diets and treatments. In a separate series of experiments, mice with cardiomyocyte-restricted deletion of insulin receptors (CIRKO) were fed a normal chow diet or a high fat diet for 36 weeks. In this study the HFD comprised 45% of calories from fat and 17% of calories from sucrose and the control diet comprised 10% of calories from fat and 7% of calories from sucrose. At the end of the experiment, the animals were euthanized; blood samples were collected; heart, fat, liver and muscles were weighed and stored at 80°C for further experimental analysis.

Human Atrial Appendage Samples. Right atrial appendage samples were obtained from diabetic and non-diabetic humans at the time of coronary artery bypass surgery from subjects described in a prior study [1].

Echocardiography. Echocardiography was performed using a Vevo 2100 imaging system from VisualSonics (Toronto, ON, Canada) with a 22-55 MHz MS550D transducer. Mice were anaesthetized with isoflurane (2% for induction and 1% for maintenance) supplemented with 100% O_2. Body temperature, respiratory rate, and ECG were constantly monitored. To minimize variation of the data, the heart rate was maintained at 450-550 beats per minute at the time when cardiac function was assessed. Cardiac function was recorded at baseline and after administration of the βAR agonist isoproterenol (ISO, 0.2 mg/kg, i.p.). Systolic function parameters including ejection

fraction (EF) and fractional shortening (FS) were measured in the two-dimensional parasternal short-axis imaging plane of M-mode tracings close to the papillary muscle level. Tissue Doppler imaging mode and pulsed-wave (PW) Doppler mode were applied to measure diastolic function as described [2, 3].

Intraperitoneal glucose tolerance test. Glucose tolerance tests were performed as described previously [4]. Briefly, mice in awake were fasted for 6h and weighed, and received an intraperitoneal injection of a glucose solution (1 mg/g i.p.). Blood samples were taken from a tail nick and glucose levels were measured using a Bayer Breeze2 standard glucometer 0, 15, 30, 60 and 120 min post injection (Bayer, Pittsburgh, PA). Area under the curve (AUC) was determined to quantify glucose intolerance.

Histology. Mice were euthanized and hearts were perfused with 4% paraformaldehyde and fixed in paraformaldehyde for 24h. Fixed hearts were then washed and stored in 70% ethanol at 4°C. Hearts were dehydrated and cleared on an Autotechnicon Mono Tissue Processor (Technicon Corporation, Tarrytown, NY), embedded in paraffin using HistoEmbedder (Leica Biosystems, Richmond, IL), and sectioned into five-micron slices using Leica RM2255 Microtomes. Tissue sections were stained with hematoxylin and eosin to examine heart morphology, and Masson's Trichrome (Sigma-Aldrich, St. Louis, MO) staining was used to quantify myocardial fibrosis. The staining was performed according to the manufacturer's protocol. For the semi quantitative analysis of collagen expression, the blue-stained areas in the sections were measured using the Image J program (NIH, Bethesda, MD, USA) by a researcher blinded to the samples. Apoptosis detection was done in fixed slices of hearts using the Promega DeadEnd™ Fluorometric TUNEL system according to manufacturer's instructions. Briefly, the slices were then permeabilized with 20 ug/mL Proteinase K and labeled with fluorescein-12-dUTP[(a)] using recombinant terminal deoxynucleotidyl transferase (rTdT). Vectashield Hard Set mounting medium with DAPI (Vector Labs) was used as the counter stain. Negative control samples were exposed to the same protocol, but lacked the rTdT enzyme treatment. Positive control samples were additionally exposed to 7.5 units/mL of DNase I (Promega) for 10 minutes at room temperature after permeabilization. The quantification was performed in six regions of each heart.

Blood insulin concentration. Plasma insulin levels were detected with an ALPCO mouse ultrasensitive insulin ELISA kit (Salem, NH) according to the manufacturer's instructions.

Cyclic AMP detection. Cyclic AMP levels in heart tissues were measured with the cAMP-Glo™ Assay kit (Promega, Madison, WI) following the manufacturer's instructions. 20 mg of heart tissue was homogenized in 500 µl chilled lysis buffer (25 mM HEPES, 0.15% Triton X-100, 150 mM NaCl, 0.5 mM IBMX, 100 µM Ro20-1724) using Lysing Matrix D Tubes (MP Biomedicals, Santa Ana, CA) using the FastPrep instrument (MP Biomedicals, Santa Ana, CA) for 40 seconds twice. The tubes were placed on ice for 5 minutes between each run. The lysates were sonicated on ice for three seconds, three times. The homogenate was centrifuged at 14,000 rpm for 15 minutes at 4 °C to eliminate tissue debris. Samples were heated for 10 minutes at 70 °C and were then

chilled on ice for 5 minutes. The samples were centrifuged to remove any precipitated proteins at 14,000 rpm at 4°C for 10 minutes. The supernatants were decanted and kept on ice and protein concentrations were measured using the Pierce BCA Protein Assay Kit (Life Technologies, Benicia, CA). The supernatants were diluted according to the protein concentration to 40 µl with lysis buffer and warmed to room temperature after which they were added into the appropriate wells of a white 96 well plate, one well was left with just lysis buffer as control. A series dilution of standard cAMP was used for the standard curve. Ten microliters of cAMP Detection Solution was added to all wells, and the plate was mixed by shaking for 2 minutes and incubated at room temperature for 20 minutes. Fifty micrograms of room temperature Kinase-Glo Reagent was added to all reactions, and the plate was mixed by shaking for 2 minutes and incubated at room temperature for 10 minutes. Relative luminescence was read on a SpectraMax M5 Multi-Mode Microplate Reader (Molecular Devices, Silicon Valley, CA) and ΔRLU was calculated by subtracting each value for each sample from that obtained with lysis buffer only. The cAMP levels are presented as ng/ug total protein.

Western blotting. Left ventricular extracts were prepared as previously described [5] in lysis buffer (25mM Tris HCl PH 7.6, 150 mM NaCl, 1% IGEPAL, 1% Sodium deoxycholate, 0.1% SDS, 1mM EDTA) with protease and phosphatase inhibitors (Na_3F 100mM, Na_2VO_4 1mM, glycerol 1mM, NaP_2O_7 2.5 mM, leupeptin 10 µg/ml, PMSF 1mM, aprotinin 10 µg/ml), and protein concentration was measured by BCA assay (Pierce, Rockford, IL). Lysates (50 µg total protein) were resolved by SDS-PAGE. The extracts were then transferred onto a PVDF membrane (Merck Millipore, Billerica, MA) and incubated with the primary antibody followed by IRDye 680CW or 800CW secondary antibodies and imaged with an Odyssey scanner (LI-COR Biosciences Lincoln, NE). The primary antibodies used for Western blotting were against following proteins: β_1AR (V-19), β_2AR (M-20), GRK2 (C-15), PDE2A (H-300), PDE5A (H-120), $G\alpha_i$ (C-10), insulin receptor-beta (C-19), IRS2 (M-19), and βarr2 (H-9) from SCBT, Santa Cruz, CA, and phospho-Akt (Ser473, #4051), AKT (#9272), phospho-MAP kinase (T202/T204, #9106), MAP kinase (p44/42, #91202), phospho-troponin (Ser23/24, #4004), troponin (#4002) from Cell Signaling, Danvers, MA, PDE3A (1098-1115, a gift from Vincent Manganiello, NIH), PDE4A (a gift from Marco Conti, University of California at San Francisco), PDE4D (ab14613, Abcam, Cambridge, MA), Serca (2A7-A1, Thermo, Rockford, IL), phospho-phospholamban (Ser16, Badrilla, London, UK), phospholamban (MA3-922, Affinity Bioreagent, Golden, CO), IRS1 (#06-248, Millipore, Billerica, MA), gamma-tubulin (T6557, Sigma-Aldrich, St Louis, MO). Signal intensity was quantitated by Image Studio software version 2.1 (LI-COR Biosciences, Lincoln, NE).

Quantitative RT/PCR. Fifty micrograms of finely minced heart tissue and 1 ml of ice-cold TRI Reagent (Sigma-Aldrich, St Louis, MO) was added to the Matrix Lysing D tube (MPbio, Santa Ana, CA). The tubes were secured in the Fast Prep machine (MPbio, Santa Ana, CA) and homogenized on speed 4.0 for 30 seconds. To ensure complete dissociation of nucleoprotein complexes, samples were allowed to stand for 5 minutes at room temperature. The TRI Reagent and sample were decanted into a 1 ml polypropylene tube after which 0.1 ml of 1-bromo-3-chloropropane was added. The sample was covered tightly, and vigorously shaken for 15 seconds, and the samples allowed to stand for

15 minutes at room temperature. The resulting mixture was then centrifuged at 12,000 × g for 15 minutes at 4 °C. The aqueous phase was then transferred to a fresh tube after which 0.5 ml of 2-propanol was added and the sample mixed. The sample was allowed to stand for 10 minutes at room temperature. Samples were centrifuged at 12,000 × g for 10 minutes at 4 °C. The RNA precipitate formed a pellet on the side and bottom of the tube. The supernatant was removed and the RNA pellet washed by adding 1 ml of 75% ethanol. The samples were vortexed and centrifuged at 7,500 × g for 5 minutes at 4 °C, after which the RNA pellet was dried for 10 minutes by air-drying. 40 µl of RNase-free water was added to dissolve the RNA pellet. All the reagents for mRNA isolation were from Sigma-Aldrich (St. Louis, MO). Messenger RNA was purified by utilizing a RNA Clean and Concentrator kit (Zymo Research, Irvine, CA) according to the manufacturer's instructions and quantified with a Synergy 2 Multi-Mode Reader (Bio-Tek, Winooski, Vermont). A260/280 reading was also performed to evaluate the purity of RNA extractions. One microgram RNA template was reverse-transcribed into cDNA by the High Capacity cDNA Reverse Transcription kit (Applied Biosystems, Foster, CA) using Applied Biosystems Veriti 96 Well Thermal Cycler. The sequence-specific primers were reconstituted and diluted to 100 nM in nuclease free water and stored at -20 °C until experimental use. All primer sequences are listed in Table 4. SYBR Advantage qPCR Premix kit (Clontech Laboratories, Inc. Mountain View, CA) was applied to measure mRNA expression according to kit directions using the ViiA™ 7 Real-Time PCR System (Life Technologies). The relative expression level of specific mRNA was determined by the comparative cycle threshold (CT) method ($2^{-\Delta\Delta CT}$), normalized to the endogenous control gene GAPDH. Each RNA sample was assayed in triplicate. The primers used in real-time PCR are listed below.

Gene	Primer	Sequences
α-MHC	F	5'-CAACGCCAAGTGTTCCTC-3'
	R	5'-AGCTCTGACTGCGACTCCTC-3'
β-MHC	F	5'-ATGTGCCGGACCTTGGAAG-3'
	R	5'-CCTCGGGTTAGCTGAGAGATCA-3'
ANP	F	5'-TCGTCTTGGCCTTTTGGCT-3'
	R	5'-TCCAGGTGGTCTAGCAGGTTCT-3'
BNP	F	5'-CTCCTGAAGGTGCTGTCC-3'
	R	5'-GCCATTTCCTCCGACTTT-3'
Col1a1	F	5'-TAGGCCATTGTGTATGCAGC-3'
	R	5'-ACATGTTCAGCTTTGTGGACC-3'
TGFβ1	F	5'-CGCCATCTATGAGAAAACC-3'
	R	5'-GTAACGCCAGGAATTGT-3'
PDE2A	F	5'-GGTGGCCTCGAAATCTGTGCTGG-3'
	R	5'-GCATGCGCTGATAGTCCTTCCG-3'
PDE3A	F	5'-CGACTCCGATTCTGACAGTG-3'
	R	5'-ATATTCCCAGACAGGCATCC-3'
PDE4A	F	5'-CTTCTGCGAGACCTGCTCCA-3'
	R	5'-GAGTTCCCGGTTCAGCATCC-3'
PDE4B	F	5'-AATGTGGCTGGGTACTCACA-3'
	R	5'-AAGGTGTCAGATGAGATTTTAAACG-3'

PDE4D	F	5’-ACCGCCAGTGGACGGACCGGA-3’
	R	5’-CATGCCACGCTCCCGCTCTCGG-3’
PDE5A	F	5’-AAATCAATTCAGTTTTGAAGATCC-3’
	R	5’-TGTTGAATAGGCCAGGGTTT-3’
GAPDH	F	5’-CATGGCCTTCCGTGTTCCTA-3’
	R	5’-CCTGCTTCACCACCTTCTTGAT-3’

Primary adult cardiomyocyte isolation and culture. The isolation of adult cardiomyocytes was carried out as described previously [5]. In brief, mice were anaesthetized with isoflurane (2%), and hearts were removed and placed in cannulation buffer (NaCl 120mM, KCl 5.4 mM, NaH_2PO_4 1.2 mM, $NaHCO_3$ 20 mM, $MgSO_4$ 1.2 mM, Glucose 5.6 mM, 2,3-Butanedione monoxime 10mM, Taurine 20mM, PH7.33. The solution was bubbled with 95% O_2 and 5% CO_2 for 10min, then filtered through a 0.22 micron filter). The heart was gently cannulated via the aorta using a small cannula attached to a 1 cc syringe and filled with cannulation buffer. After perfusing with the cannulation buffer for 4 minutes (3 ml per minute) and when there was about 10 ml buffer remaining in reservoir, 5 ml collagenase solution (containing 2.5 mg type II collagenase (Worthington Biochemical, Lakewood, NJ), 0.5 mg type XIV protease (Sigma-Aldrich) and 0.1 % BSA, filtered) was added into buffer for pre-digestion. Then the perfusion was continued with 20 ml of a fresh collagenase solution (containing 10 mg type II collagenase, 2 mg type XIV protease, 50 μM $CaCl_2$, 0.1 % BSA, filtered), which was recirculated to maintain perfusion for approximately 12-16 minutes until the heart became soft. The heart was cut below the atria into a dish containing 5 ml of collagenase solution with calcium, cut 5-10 times and transferred into a 15 ml tube. The supernatant was transferred into a new tube with 5 ml stopping buffer (12.5 μM $CaCl_2$ and 0.5 ml FBS), and centrifuged at 500 rpm for 1 minute, and repeated up to 2 times to ensure digestion. The cell pellet was resuspended and recovered in gradient calcium buffer to a physiological concentration (1mM). For myocyte cultures, the cell number was counted and 50,000 /ml cell was plated on natural mouse laminin (Life Technologies, Grand Island, NY) coated dishes with M1018 media (10.7 g Sigma M1018 Minimum Essential Medium Eagle, 0.35 g NaCHO3, 1% Penicillin-Streptomycin, PH 7.4, filtered).

Fluorescence resonance energy transfer (FRET) measurements. Adult rat cardiomyocytes were cultured on glass coverslips and infected with regular ICUE3, an Epac based cAMP biosensor for 36 h. Coverslips with living myocytes were treated with insulin 100 nM, overnight in media and then maintained in PBS w/o calcium (KCl 2.68 mM, KH_2PO_4 1.47 mM, NaCl 136.89 mM, Na_2HPO_4 8.1 mM) for FRET recording as described previously [6]. Images were acquired using a Leica DMI3000 B inverted fluorescence microscope (Leica Biosystems, Buffalo Grove, IL) with a 40×/1.3 numerical aperture oil-immersion objective lens and a charge-coupled device camera controlled by Metafluor software (Molecular Devices, Sunnyvale, CA). FRET was recorded by exciting the donor fluorophore at 430-455 nm and measuring emission fluorescence with two filters (475DF40 for cyan and 535DF25 for yellow). Images were subjected to background subtraction, and were acquired every 20 seconds with exposure time of 200

Ms. The donor/acceptor FRET ratio was calculated and normalized to the ratio value of baseline. The binding of cAMP to ICUE3 decreased CFP–YFP FRET efficiency.

Adult cardiomyocyte contractility and calcium transient. Freshly isolated adult cardiomyocytes were loaded with Fluo-4 AM (5 μM; Molecular Probes, Grand Island, NY,) for 30 min. Cells were then placed in the middle of a glass-bottomed dish with 3 ml beating buffer (NaCl 120 mM, KCl 5.4 mM, NaH_2PO_4 1.2 mM, $MgSO_4$ 1.2 mM, HEPES 20 mM, Glucose 5.5 mM, $CaCl_2$ 1mM, PH 7.1, filtered) and settled for 5 minutes. Platinum electrodes were placed near the cell and paced at 1 Hz with voltage of 30 V using the SD9 stimulator (Grass Technology, Warwick, RI) as described [7]. The calcium transient and contractile events of myocytes were recorded on an inverted microscope (Zeiss AX10, Dublin, CA) at 20× magnification enabling observation of 5-10 rod-shaped cardiomyocytes with clear striations per field of view using the Metamorph program (Molecular Devices, Sunnyvale, CA). The following settings were applied: time interval 1 minute, duration 10 minutes, 200 frames per movie, exposure time 25 ms, movie length 5 seconds. Drugs (Rolipram 100nM, ISO 100 nM) were added into the dish after two movies were acquired. The percentage of myocyte fractional shortening (FS) was calculated as (maximal cell length – minimal cell length)/ maximal cell length × 100%. The analysis was performed by Metamorph. The calcium transient were recorded with excitation at 488 nm and emission collected at >505 nm. Analysis was made using a homemade routine in interactive data language (ITT) as previously described [8].

Statistical analysis. All data are expressed as mean ± SEM. All statistical analysis was performed using GraphPad Prism 6 software (La Jolla, CA). The sample size for each group is shown in the figure legends or tables. The *in vitro* studies were done with at least three sets of independent experiments. Differences between two groups were evaluated by 2 -tailed Student's *t*-test; comparisons of multiple groups were performed using either one-way or two-way ANOVA followed by post hoc Tukey's test. $P < 0.05$ was defined as statistically significant.

1. Anderson EJ, Kypson AP, Rodriguez E, Anderson CA, Lehr EJ and Neufer PD. Substrate-specific derangements in mitochondrial metabolism and redox balance in the atrium of the type 2 diabetic human heart. *J Am Coll Cardiol*. 2009;54:1891-8.
2. Qi Y, Xu Z, Zhu Q, Thomas C, Kumar R, Feng H, Dostal DE, White MF, Baker KM and Guo S. Myocardial loss of IRS1 and IRS2 causes heart failure and is controlled by p38alpha MAPK during insulin resistance. *Diabetes*. 2013;62:3887-900.
3. Zhang X, Szeto C, Gao E, Tang M, Jin J, Fu Q, Makarewich C, Ai X, Li Y, Tang A, Wang J, Gao H, Wang F, Ge XJ, Kunapuli SP, Zhou L, Zeng C, Xiang KY and Chen X. Cardiotoxic and cardioprotective features of chronic beta-adrenergic signaling. *Circ Res*. 2013;112:498-509.
4. Sloan C, Tuinei J, Nemetz K, Frandsen J, Soto J, Wride N, Sempokuya T, Alegria L, Bugger H and Abel ED. Central leptin signaling is required to normalize myocardial fatty acid oxidation rates in caloric-restricted ob/ob mice. *Diabetes*. 2011;60:1424-34.

5. Fu Q, Xu B, Liu Y, Parikh D, Li J, Li Y, Zhang Y, Riehle C, Zhu Y, Rawlings T, Shi Q, Clark RB, Chen X, Abel ED and Xiang YK. Insulin inhibits cardiac contractility by inducing a Gi-biased beta2-adrenergic signaling in hearts. *Diabetes*. 2014;63:2676-89.
6. Soto D, De Arcangelis V, Zhang J and Xiang Y. Dynamic protein kinase a activities induced by beta-adrenoceptors dictate signaling propagation for substrate phosphorylation and myocyte contraction. *Circ Res*. 2009;104:770-9.
7. Fu Q, Xu B, Parikh D, Cervantes D and Xiang YK. Insulin induces IRS2-dependent and GRK2-mediated beta2AR internalization to attenuate betaAR signaling in cardiomyocytes. *Cell Signal*. 2015;27:707-15.
8. Pereira L, Cheng H, Lao DH, Na L, van Oort RJ, Brown JH, Wehrens XH, Chen J and Bers DM. Epac2 mediates cardiac beta1-adrenergic-dependent sarcoplasmic reticulum Ca2+ leak and arrhythmia. *Circulation*. 2013;127:913-22.

Supplementary Figure Legends for:

Inhibiting insulin-mediated β_2AR activation prevents diabetes-associated heart failure.

Author list:
Qingtong Wang, Yongming Liu, Qin Fu, Bing Xu, Yuan Zhang, Sungjin Kim, Ruensern Tan, Federica Barbagallo, Toni West, Ethan Anderson, Wei Wei, E. Dale Abel, and Yang K. Xiang.

Supplementary Figure 1. Characterization of metabolic profiles in HFD mice. a) Plasma glucose and insulin levels were measured in HFD- and NC-fed mice after a 6-hour fast (n=12). b) After 6 months of HFD GTT was performed on HFD- and NC-fed mice (n=12). Time course of plasma glucose levels after IP glucose injection (1g/kg, left); the area under the curve (AUC) was plotted (right). $^{\#}p < 0.05$ and $^{\#}p < 0.001$ by student *t*-test between paired groups. c) 6 months of HFD decreases protein levels of IRβ and IRS2, but increases phosphorylation of S6K1 (T389) and GSK3 (S9) in mouse hearts (n=12). ** $p < 0.01$ and *** $p < 0.001$ by student *t*-test between paired groups. d) Insulin (100 nM) induces activation of ERK (T202/Y204) and Akt (S473) in myocytes isolated from NC and HFD hearts (N = 3). * $p < 0.05$ and ** $p < 0.01$ by one-way ANOVA followed by post hoc Tukey's test.

Supplementary Figure 2. Cardiac tissue characterization of HFD-fed wildtype mice. a) Heart sections from HFD- and NC-fed mice were stained with hematoxylin and eosin to examine heart morphology, Masson's Trichrome to examine fibrosis, and TUNEL staining to examine apoptosis, respectively (n=4). Wall thickness of left ventricle, fibrosis, and apoptosis were quantified and plotted. b) mRNA levels were measured from

heart lysates in HFD- and NC-fed mice (n=12). $^{\#}p< 0.05$, $^{\#\#}$ $p < 0.01$, and $^{\#\#\#}$ $p < 0.001$ by student *t*-test between paired groups.

Supplementary Figure 3. Characterization of the insulin-induced transactivation of β_2AR-β-arrestin2-ERK pathway in cardiac myocytes. a) Insulin (100 nM, 5 minutes) promotes formation of a β_2AR-β-arrestin2-ERK complex in AVMs (N=3). * $p < 0.05$ by student *t*-test between paired groups. b) Insulin-induced ERK activation and PDE4D expression in AVMs from WT and β_1KO mice (n=3). * $p < 0.05$ by student *t*-test between paired groups. c) Insulin (100nM)-induced ERK activation (30 minutes) and PDE4D expression (12hrs) in mouse AVMs is blocked by a GRK2 inhibitor paroxetine (Parox, 100μM), but not by fluoxetine (Fluox 100μM, n=5). * $p< 0.05$ by one-way ANOVA followed by post hoc Tukey's test. d) Insulin (100nM)-induced ERK activation (30 minutes) and PDE4D expression (12 hours) in mouse AVMs is attenuated by β-blocker carvedilol (100 nM) and timolol (1μM). * $p< 0.05$ by one-way ANOVA followed by post hoc Tukey's test.

Supplementary Figure 4. Characterization of metabolic profiles in HFD-fed β_2AR-KO and β-arrestin2-KO mice. a and b) Plasma glucose and insulin levels were measured in HFD- and NC-fed mice after a 6-hour fast (n=12). c) After 6 months of HFD, GTT was performed on HFD and NC-fed mice (n=12). Time course of plasma glucose levels after IP of glucose (1g/kg, left); the area under the curve (AUC) was plotted (right). $^{*}p< 0.05$, ** $p < 0.01$, and *** $p < 0.001$ by student *t*-test between paired groups.

Supplementary Figure 5. Cardiac tissue characterization of HFD-fed β_2AR-KO and β-arrestin2-KO mice. a and b) Heart sections from HFD- and NC-fed mice were stained with hematoxylin and eosin to examine heart morphology, Masson's Trichrome to examine fibrosis, and TUNEL staining to examine apoptosis, respectively (n=12). Wall thickness of left ventricle, fibrosis, and apoptosis were quantified and plotted. c and d) mRNA levels were measured from heart lysates in HFD- and NC-fed mice. $^{\#}p< 0.05$ and $^{\#\#}p < 0.01$ by student *t*-test between paired groups. $^{*}p< 0.05$, ** $p < 0.01$, and *** $p < 0.001$ by one-way ANOVA followed by post hoc Tukey's test.

Supplementary Figure 6. Characterization of gene expression in HFD cardiac tissues. a) mRNA levels were measured from heart lysates in HFD- and NC-fed β_2AR-KO mice (n=12). b) mRNA levels were measured from heart lysates in HFD- and NC-fed β-arrestin2-KO mice (n=12). c) mRNA levels were measured from heart lysates in HFD- and NC-fed mice after drug therapies (n=12). *$p< 0.05$ and **$p < 0.01$ by student *t*-test between paired groups.

Supplementary Figure 7. Metabolic characterization of HFD-fed mice after treatment with paroxetine and carvedilol. a) After 4 months of HFD, mice were treated with vehicle, paroxetine (2.5 mg/kg body weight) or carvedilol (2.5 mg/kg body weight) for 4 weeks. Plasma glucose and insulin levels were measured in HFD- and NC-fed mice after a 6-hour fast (n=12). b). GTT was conducted on HFD and NC-fed mice after a 6-hour fast (n=12). Time course of plasma glucose levels after IP injection of glucose (1g/kg,

left); the area under curve (AUC) was plotted (right). *p< 0.05 and *** p < 0.001 by one-way ANOVA followed by post hoc Tukey's test.

Supplementary Figure 8. Cardiac tissue characterization of HFD-fed mice after treatment with paroxetine and carvedilol. a and b) Heart sections from HFD- and NC-fed mice were stained with hematoxylin and eosin to examine heart morphology and Masson's Trichrome to examine fibrosis, and TUNEL staining to examine apoptosis, respectively (n=4). Wall thickness of the left ventricle, fibrosis, and apoptosis were quantified and plotted. c) mRNA levels were measured from heart lysates in HFD- and NC-fed mice (n=12). * p< 0.05, ** p < 0.01, and *** p < 0.001 by one-way ANOVA followed by post hoc Tukey's test.

Supplemental Figure 1

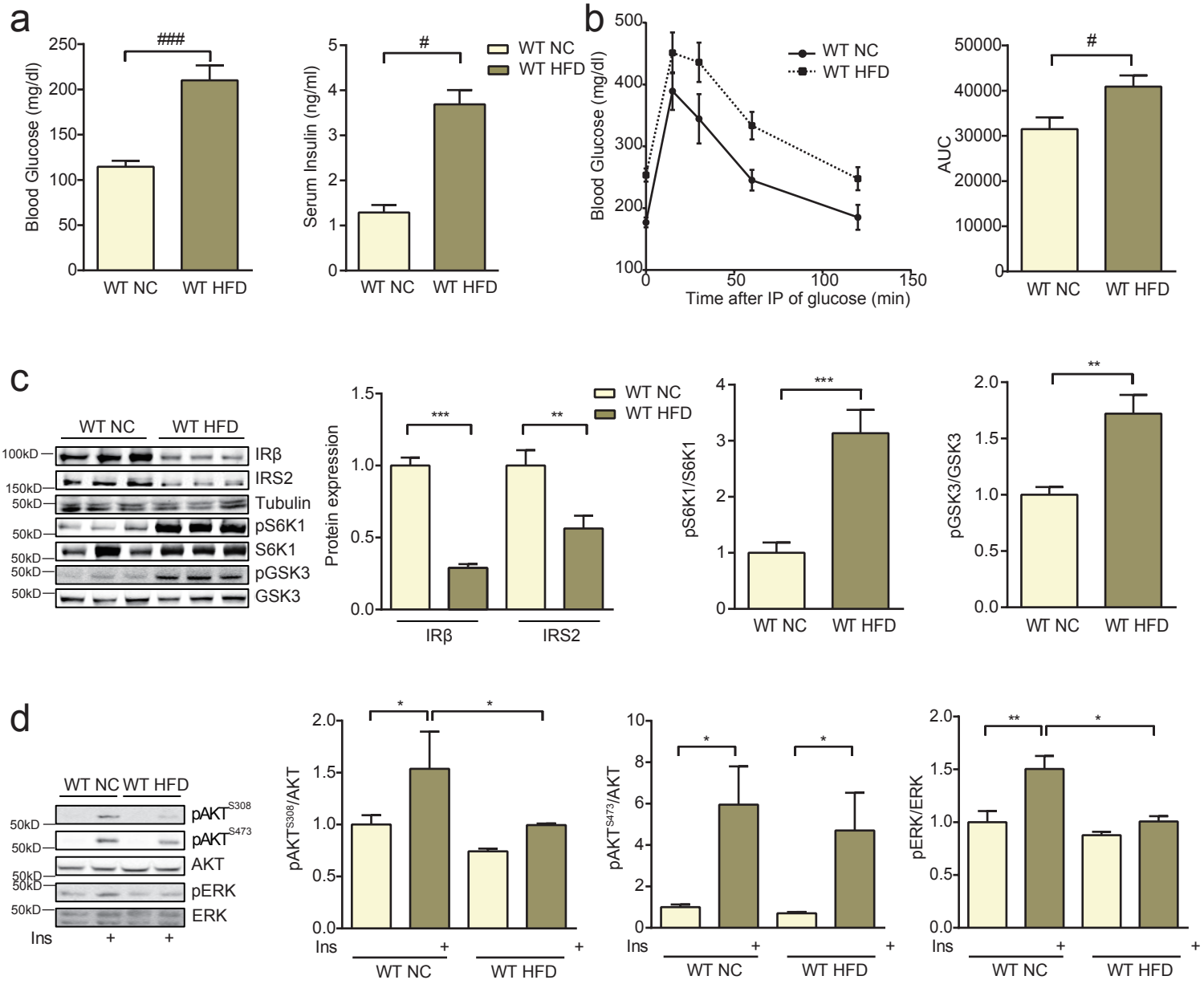

Supplemental Figure 2

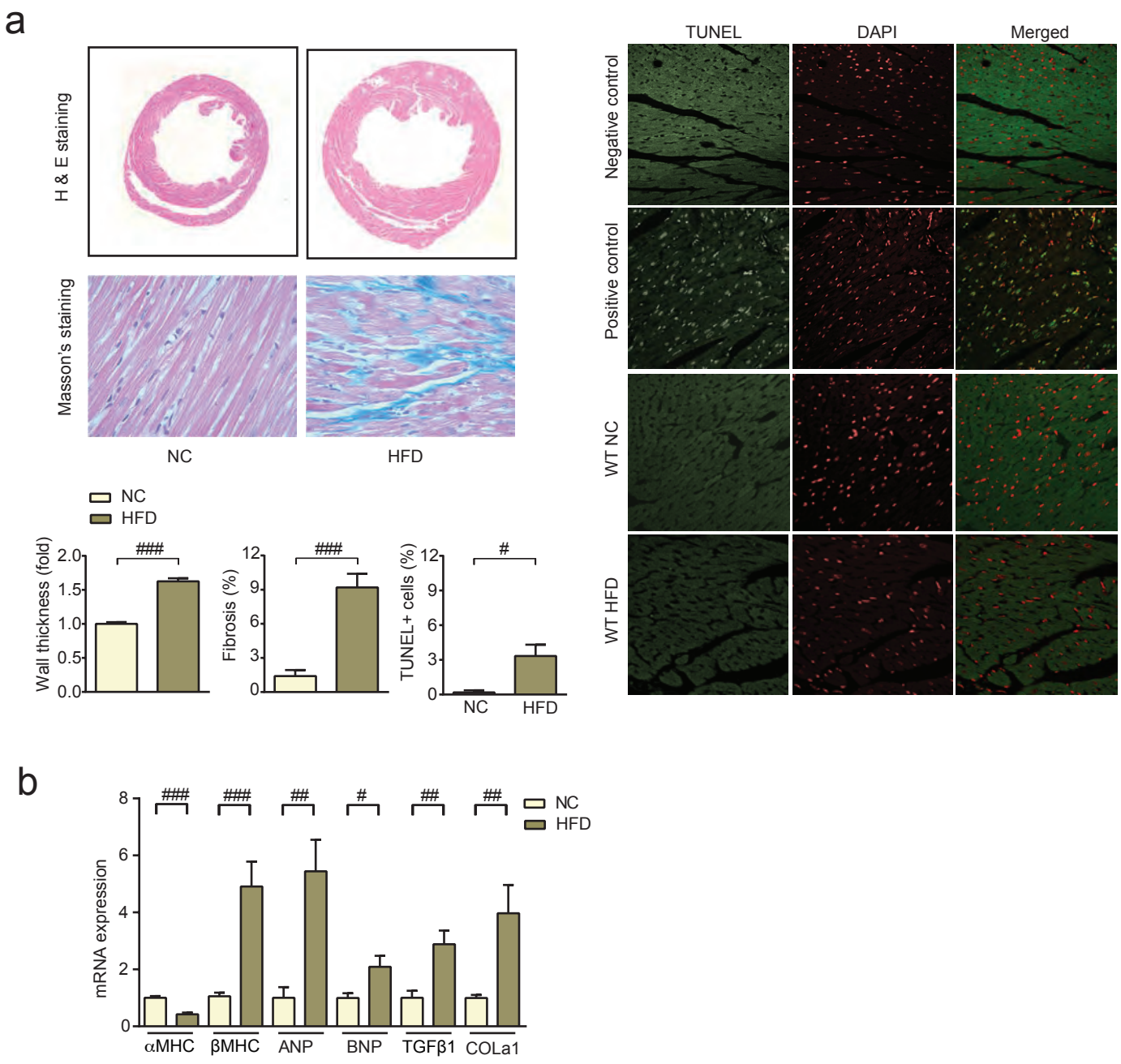

Supplementary Figure 3

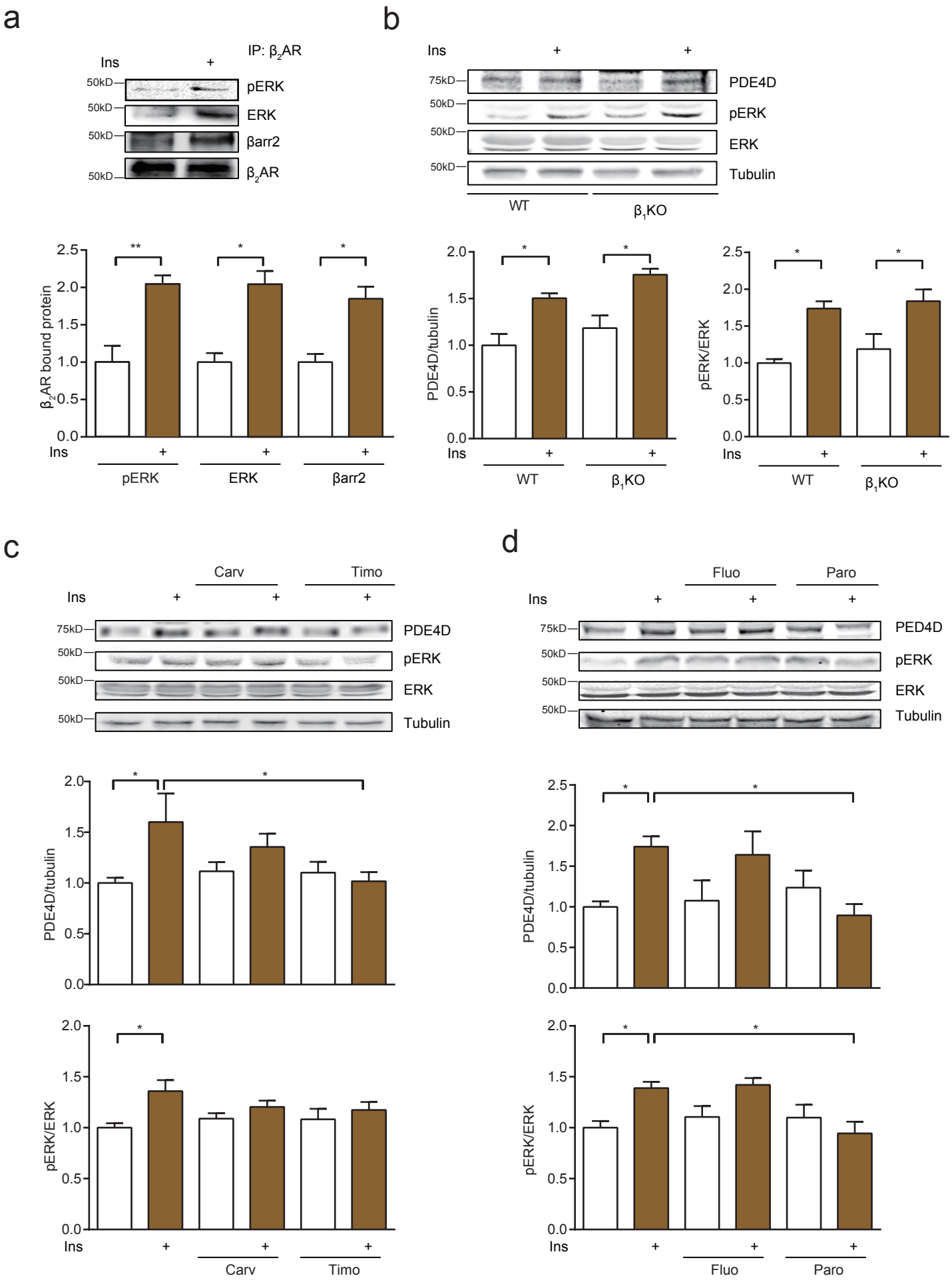

Supplemental Figure 4

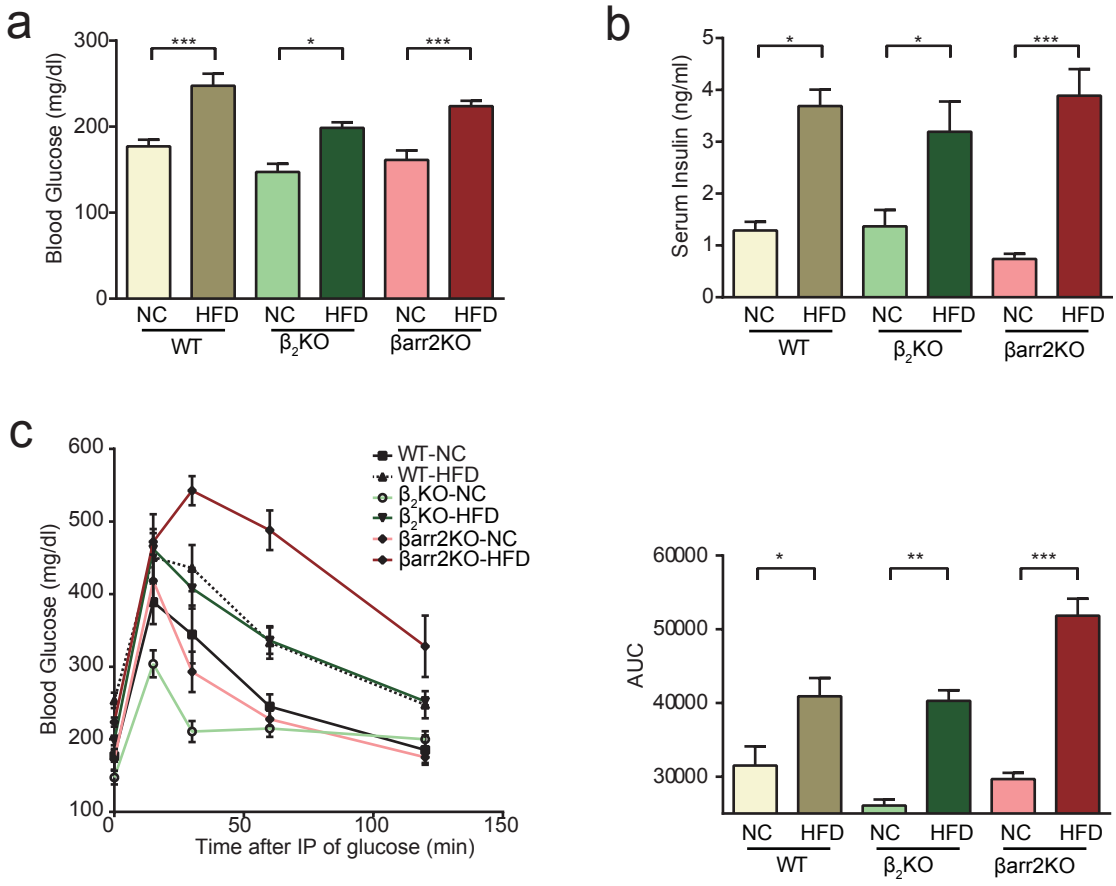

Supplemental Figure 5

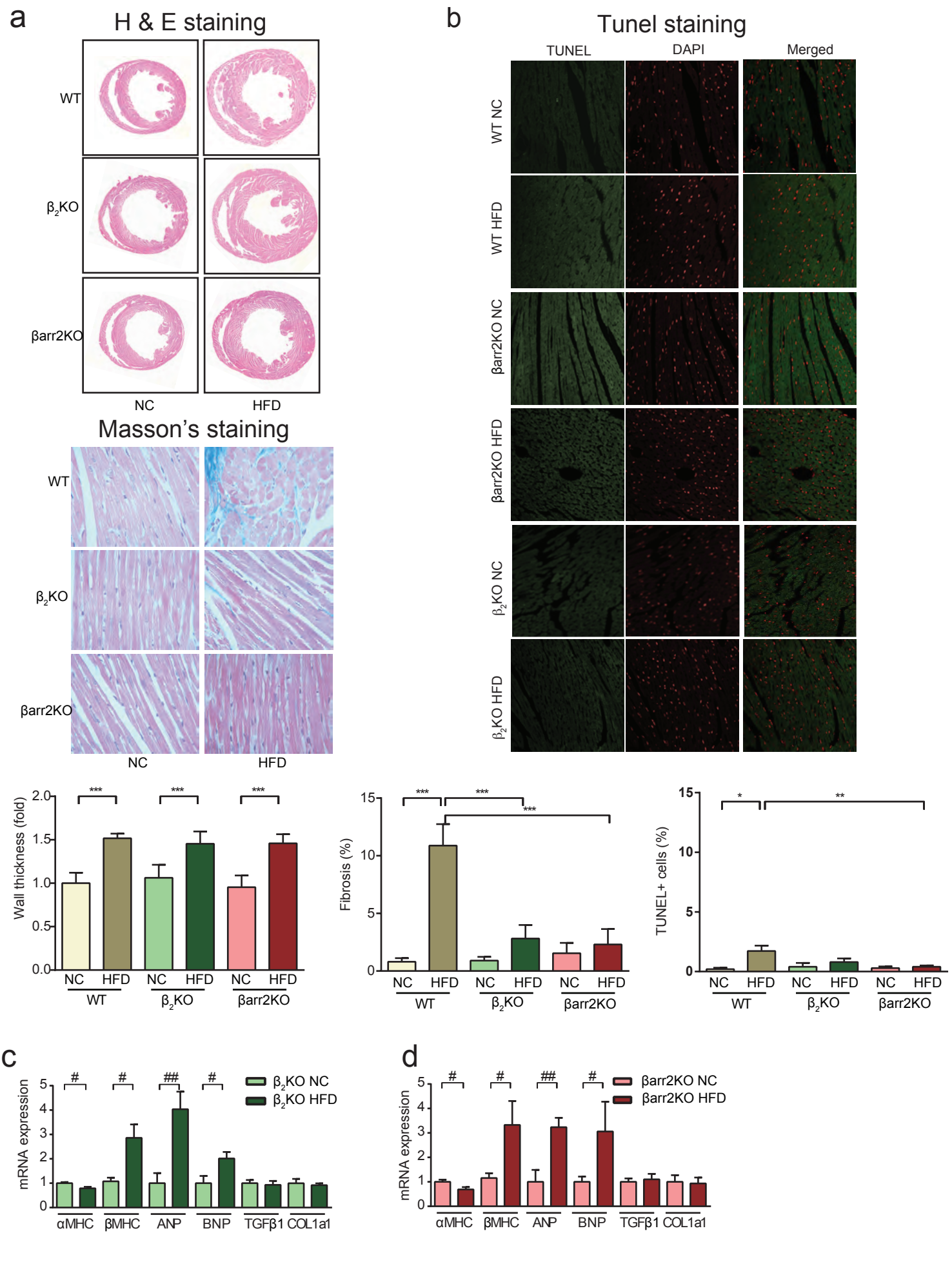

Supplemental Figure 6

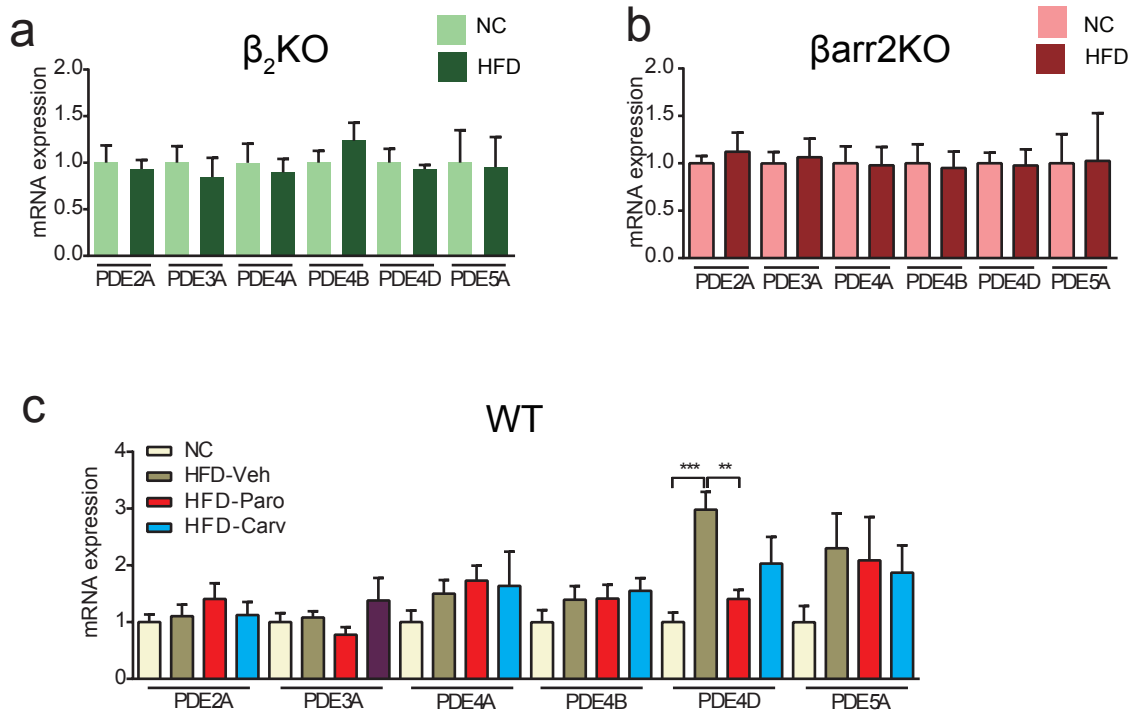

Supplemental Figure 7

a

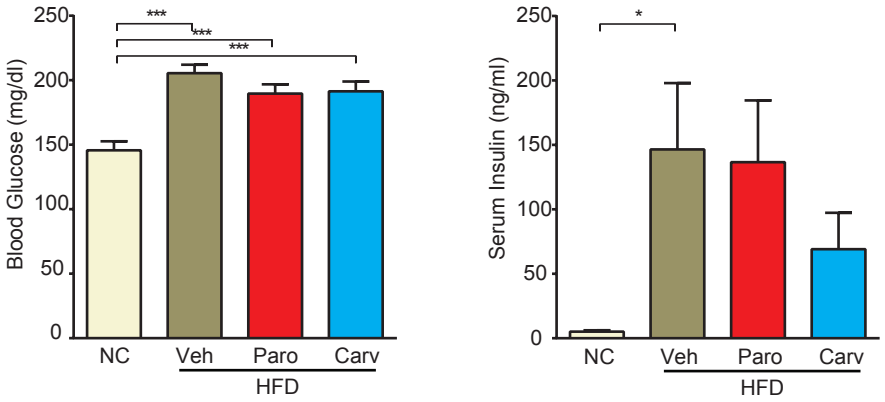

b

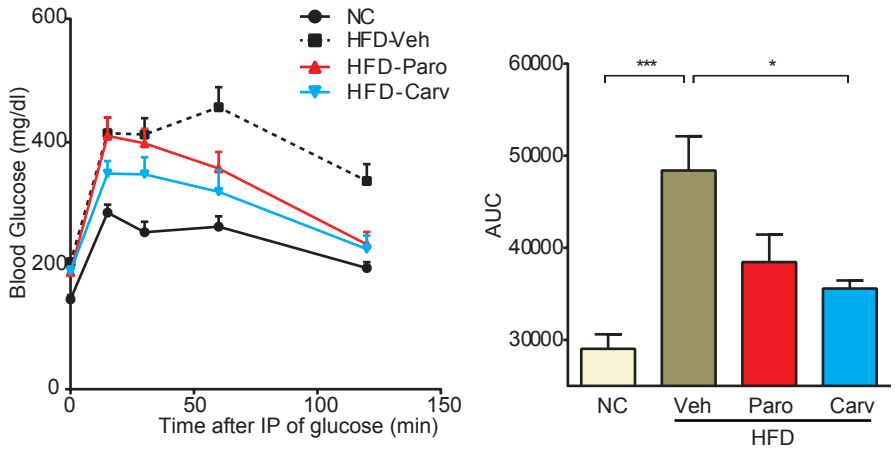

Supplemental Figure 8

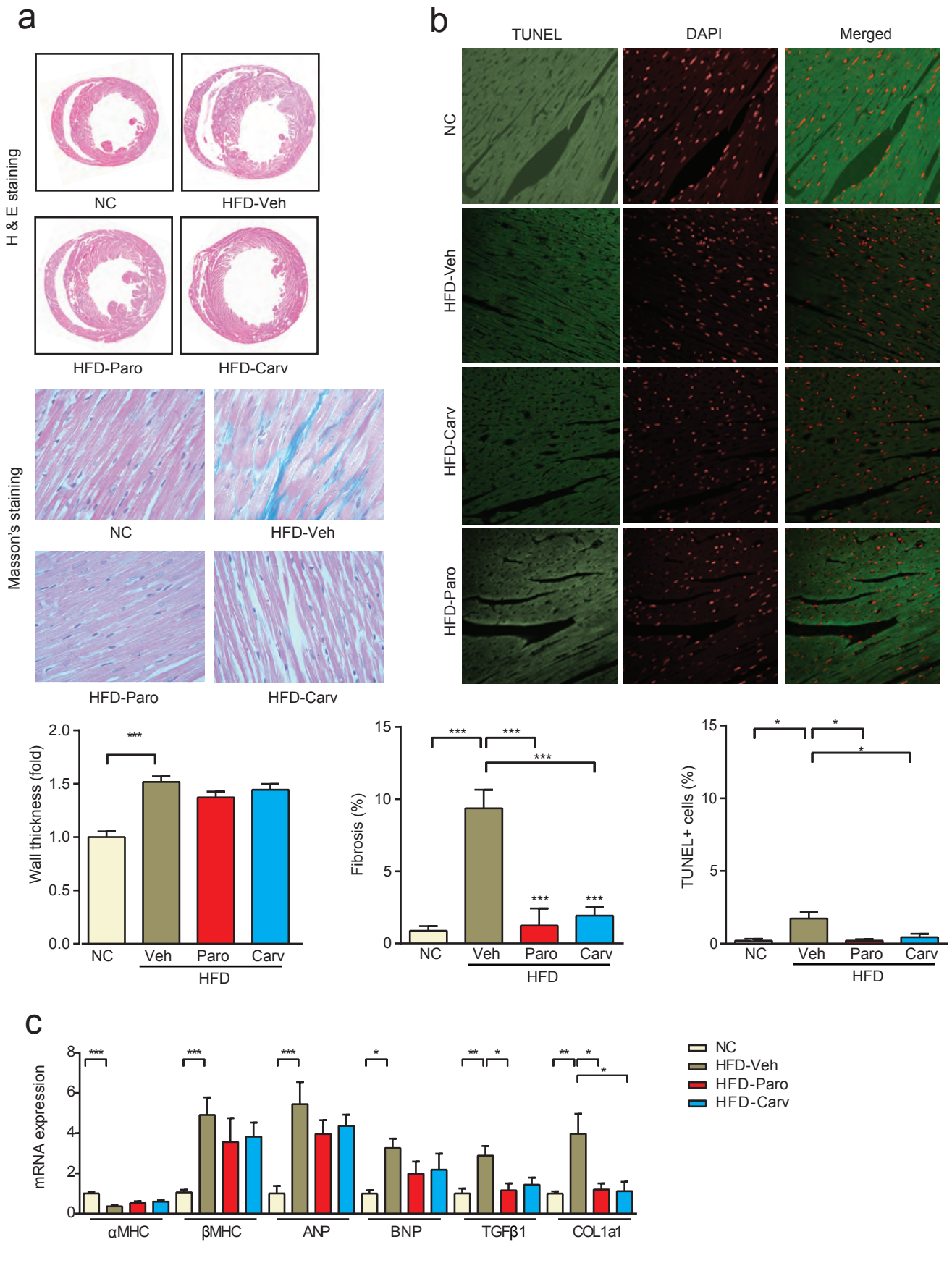

Supplemental Table 1. Echo data of WT mice of 6 months' high fat feeding (mean±SEM)

	NC	HFD
HR	466.4±6.153	435.0±21.87
IVS d(mm)	0.6318±0.02536	0.6881±0.05523
IVS s(mm)	0.9639±0.03162	0.9404±0.08069
LVID; d(mm)	3.841±0.06359	4.054±0.1472
LVID; s(mm)	2.853±0.05864	3.281±0.1291$^{\#\#}$
LVPW; d(mm)	0.7191±0.03534	0.7854±0.03776
LVPW; s(mm)	0.9212±0.03767	0.9676±0.04710
EF %	52.16±0.7499	39.55±2.891$^{\#\#\#}$
FS %	26.25±0.4707	19.04±1.601$^{\#\#\#}$
LV Mass (mg)	88.24±4.952	109.4±12.21
Mass (corre)	70.59±3.962	87.52±9.770
LV Vol; d(uL)	63.75±2.514	72.99±6.123
LV Vol; s(uL)	31.13±1.568	44.05±4.177$^{\#\#}$
A'	-18.08±0.8494	-17.14±1.685
E'	-19.07±0.8388	-15.47±2.163$^{\#\#\#}$
ET	46.29±1.095	46.13±2.813
IVCT	17.69±1.079	21.08±2.331
IVRT	14.77±0.6579	24.57±1.099$^{\#\#\#}$
MPI[(IVRT+IVCT)/ET]	0.7084±0.04848	1.002±0.05992$^{\#\#}$
A'/E'	0.9564±0.04641	1.346±0.1302$^{\#\#}$
E'/A'	1.065±0.04972	0.7711±0.07352$^{\#\#}$
MV A(mm/s)	400.2±16.95	313.3±36.97$^{\#}$
MV E(mm/s)	751.8±44.31	381.5±31.04$^{\#\#\#}$
MV E/A	1.873±0.05027	1.275±0.06518$^{\#\#\#}$
E/E'	-40.17±3.531	-30.29±3.412
Vcf=FS/ET	0.5578±0.01776	0.4215±0.04441$^{\#\#}$

$^{\#}P<0.05$, $^{\#\#}P<0.01$, $^{\#\#\#}P<0.001$ WT HFD *vs* WT NC group; IVS d: intact ventricular septum end diastole; IVS s: intact ventricular septum end systole; LVID d: Left ventricular internal diameter end diastole and end diastole; LVID s: Left ventricular internal diameter end diastole and end systole; LVPW d Left ventricular posterior wall end diastole; LVPW s Left ventricular posterior wall end systole; EF, ejection fraction; FS, fractional shortening; LV Mass, left ventricular mass; Mass (corre), corrected LV mass; LV Vol d, left ventricular volume end diastole; LV Vol s, left ventricular volume end systole; A', late diastolic mitral annular velocities; E', early diastolic mitral annular velocities; ET, ejection time; IVCT, isovolumic contraction time; IVRT, isovolumetric relaxation time; MPI, myocardial performance index; MV A, mitral valve A; MV E, mitral valve E; E/E', relationship between maximal values of passive mitral inflow (E) and lateral early diastolic mitral annular velocities (E'); Vcf, mean velocity of LV shortening through the minor axis.

Supplemental Table 2 Tissue weight of WT, β_2KO and βarr2KO mice of 6 months' high fat feeding (mean±SEM)

Groups	Body weight (g)	Brain weight (mg)	Heart weight (mg)	Liver weight (g)	Muscle weight (mg)	Fat weight (g)	Tibia length (cm)	Heart/Tibia (mg/cm)
WT NC	37.74±0.47	420.60±12.60	133.20±5.56	1.42±0.06	56.59±1.04	2.01±0.10	2.33±0.03	57.16±2.09
WT HFD	54.28±1.28***	415.10±8.60	154.80±4.22*	3.15±0.22***	60.29±1.79	4.04±0.19***	2.33±0.03	66.55±1.46**
β_2KO NC	34.69±0.87	423.80±4.94	135.50±2.88	1.27±0.08	53.22±0.93	1.68±0.15	2.32±0.02	58.34±1.28
β_2KO HFD	57.45±1.35$^{@@@}$	415.00±8.74	155.70±3.37$^{@@}$	4.03±0.14$^{@@@\$\$\$}$	56.47±1.09	4.18±0.22$^{@@@}$	2.31±0.02	67.77±1.67$^{@@@}$
βarr2KO NC	31.49±1.22$^{\Delta}$	450.80±6.06	143.80±3.52	1.02±0.05	55.16±0.73	0.82±0.18$^{\Delta\Delta}$	2.37±0.03	60.66±1.56
βarr2KO HFD	48.44±1.53$^{@@@\$}$	436.30±9.35	158.90±6.33	1.82±0.15$^{@\$\$\$}$	54.71±1.44	3.90±0.09$^{@@@}$	2.34±0.02	69.67±2.22$^{@}$

**P<0.05, **P<0.01, ***P<0.001* WT HFD *vs* WT NC group; $^{@}$*P<0.05,* $^{@@}$*P<0.01,* $^{@@@}$*P<0.001* β_2KO HFD *vs* β_2KO NC group or βarr2KO NC *vs* βarr2KO HFD; $^{\$}$*P<0.05,* $^{\$\$\$}$*P<0.001* β_2KO HFD or βarr2KO HFD *vs* WT HFD group, $^{\Delta}$*P<0.05,* $^{\Delta\Delta}$*P<0.01* βarr2KO NC *vs* WT NC group.

Supplemental Table 3. Echo data of Paroxetine treatment mice (mean±SEM)

	NC		HFD					
			Vehicle		Paroxetine		Carvedilol	
	16W	20W	16W	20W	16W	20W	16W	20W
HR	466.40±6.15	490.70±19.37	455.05±11.87	447.70±10.77	452.83±9.42	535.50±14.44$^{@@@}$	460.38±6.35	438.80±14.31
IVS d(mm)	0.63±0.03	0.71±0.03	0.71±0.02	0.81±0.05	0.69±0.02	0.79±0.03	0.69±0.03	0.74±0.03
IVS s(mm)	0.94±0.04	1.22±0.06	1.04±0.04	1.09±0.06	1.03±0.04	1.25±0.04	1.01±0.07	1.25±0.05
LVID; d(mm)	3.86±0.07	4.22±0.09	3.90±0.04	3.97±0.10	3.87±0.06	3.99±0.06	3.83±0.08	4.07±0.08
LVID; s(mm)	2.86±0.07	3.09±0.06	2.97±0.05	3.18±0.09	2.95±0.06	2.78±0.07$^{@@}$	2.88±0.09	2.89±0.07$^{@}$
LVPW; d(mm)	0.70±0.04	0.77±0.03	0.97±0.04***	0.88±0.03	0.95±0.03***	0.83±0.03	0.99±0.07***	0.78±0.02
LVPW; s(mm)	0.94±0.05	1.15±0.05	1.28±0.03***	1.04±0.03	1.19±0.02***	1.22±0.04$^{@}$	1.22±0.06***	1.22±0.04$^{@}$
EF %	51.77±1.67	54.27±1.50$^{@@@}$	47.23±1.52*	43.11±1.74	47.08±1.37*	58.04±1.86$^{@@@}$	47.10±1.47*	57.36±1.47$^{@@@}$
FS %	25.91±0.86	27.95±1.03$^{@@@}$	23.35±0.90*	21.03±0.98	23.85±0.77*	30.46±1.27$^{@@@}$	23.55±0.73*	29.93±1.00$^{@@@}$
LV Mass (mg)	87.25±4.16	115.60±3.54	121.9±3.06***	125.60±7.48	116.0±2.29***	120.40±6.33	118.2±2.25***	113.50±4.96
Mass (corre)	69.80±3.33	92.48±2.83	91.21±3.04***	100.50±5.99	94.12±1.79***	96.33±5.07	96.07±4.08***	90.81±3.97
LV Vol; d(uL)	64.48±2.56	80.12±4.10	66.09±1.64	69.91±4.16	64.57±2.74	69.94±2.29	67.40±1.54	73.59±3.55
LV Vol; s(uL)	31.20±1.98	37.92±1.92	34.55±1.27	41.15±2.86	33.43±1.96	29.51±1.84$^{@@}$	35.00±1.12	32.51±2.09$^{@}$
A'	-17.85±1.26	-19.34±1.24	-15.01±0.87	-18.03±1.37	-15.58±1.17	-20.21±1.85	-15.51±1.33	-17.05±1.11
E'	-18.72±0.66	-20.01±1.96$^{@}$	-12.74±0.87***	-13.33±0.76	-12.21±1.06***	-19.76±1.61$^{@}$	-12.10±1.03***	-17.96±1.59
ET	45.58±1.01	46.72±1.24	44.70±0.94	47.32±1.83	44.33±1.25	44.69±0.71	45.24±1.09	48.52±1.22
IVCT	17.20±0.95	19.78±1.22	21.20±0.94*	20.24±1.00	20.83±1.06*	18.76±0.80	22.04±1.28*	17.89±0.99
IVRT	14.75±0.69	17.64±1.27$^{@}$	24.01±1.25***	23.55±1.38	24.33±1.44***	18.41±1.18$^{@}$	25.46±2.01***	18.93±1.14$^{@}$
MPI[(IVRT+IVCT)/ET]	0.71±0.05	0.81±0.04	1.017±0.04***	0.94±0.05	1.064±0.05***	0.83±0.04	1.055±0.05***	0.77±0.04$^{@}$
A'/E'	0.95±0.04	1.02±0.06$^{@@}$	1.18±0.05*	1.41±0.05	1.28±0.08*	1.04±0.06$^{@@}$	1.28±0.07*	1.05±0.09$^{@@}$
E'/A'	1.05±0.05	1.03±0.06$^{@@}$	0.85±0.04*	0.72±0.02	0.78±0.07*	1.01±0.06$^{@@}$	0.78±0.06*	0.96±0.07$^{@}$
MV A(mm/s)	385.40±7.06	335.50±27.21	346.40±25.72	335.40±25.09	328.60±35.79	304.60±23.45	331.70±22.45	282.90±19.81
MV E(mm/s)	713.70±29.85	632.90±35.43$^{@@@}$	473.00±5.04***	432.40±36.81	450.00±40.51***	551.90±27.87$^{@}$	449.30±37.63***	527.90±25.56
MV E/A	1.851±0.06	1.96±0.09$^{@@@}$	1.37±0.02***	1.32±0.05	1.37±0.04***	1.90±0.08$^{@@@}$	1.35±0.04***	1.94±0.08$^{@@@}$
E/E'	-38.32±1.76	-35.55±3.27	-36.48±2.93	-33.05±2.81	-34.47±3.56	-30.76±2.79	-37.34±3.53	-32.41±2.80
Vcf=FS/ET	0.57±0.02	0.66±0.04$^{\#}$	0.53±0.01	0.47±0.03	0.54±0.02	0.71±0.03$^{@@@}$	0.52±0.02	0.70±0.05$^{@@}$

**P<0.05, **P<0.01, ***P<0.001* HFD, Paroxetine, Carvedilol 16W *vs* NC 16W; $^{@}$*P<0.05,* $^{@@}$*P<0.01,* $^{@@@}$*P<0.001* 20W *vs* 16W.